Fabrication of advanced titanium dioxide nanotubes.

Lyndon Leong

Bachelor of Engineering

Mechanical Engineering

Department of Mechanical Engineering

Macquarie University

November 7, 2016

Supervisor: Dr Yijiao Jiang

Statement of Candidate

I, Lyndon Leong, declare that this report, submitted as part of the requirement for the award of Bachelor of Engineering in the Department of Mechanical Engineering, Macquarie University, is entirely my own work unless otherwise referenced or acknowledged. This document has not been submitted for qualification or assessment an any academic institution.

Student's Name: Lyndon Leong

Student's Signature: LLeong

Date: 6/11/16

Acknowledgments

I would like to acknowledge Dr Yijiao Jiang for her guidance through this thesis project. I would also like to thank Yuxiang Zhu for taking time out of her schedule to helping me throughout this project and in the lab, Mr Yimin Xie for helping me with the coding for the Programmable power supply. Nichole Vella for helping and instructing me with work involving FESEM imagery which was performed in-part at the OptoFab node of the Australian National Fabrication Facility, utilising NCRIS and NSW state government funding.

Abstract

Titanium dioxide nano-tube arrays can be synthesised through different methods such as hydrothermal synthesis and electrolytic anodization. Self-organised titanium dioxide nano-tube where synthesised through a process of anodization. The specific properties of the titanium dioxide nano-tube where changed through the modification of the fabrication process such as changes to electrolyte and the addition of metal deposition. The crystalline structure of the self-organized titanium dioxide nano-tube arrays was then altered in an annealing process.

Titanium dioxide has many applications such as solar energy generation or use as a photo catalyst. By arranging structure of Titanium dioxide in the form of tubes the effectiveness of its ability in use as a photo catalyst increases. This paper looks at how titanium dioxide nanotubes arrays being used in as a photo catalyst. The structure of titanium dioxide nanotube arrays where then optimised and adjusted to increase the photocatalytic effectiveness in degradation of a common pollutant Rhodamine B. Rhodamine B was diluted into distilled water and placed in a photocatalytic chamber with a sample of foil with the Titanium Dioxide nanotube arrays and illuminated with a 300w Xeon lamp, the degradation recorded.

Table of Contents

Statement of Candidate 2
Acknowledgments 4
Abstract 6
Table of Contents 7
List of Figures 9
List of Tables 10
Introduction. 11
Literature review 12
- Electrolysis 12
- Titanium Dioxide Nanotube Arrays 13
  - Formation 13
  - Modification 15
- Cadmium Sulphide Sensitization. 19
- NiO/N-doped TNTs. 20
- Applications 21
  - Photovoltaics 21
  - Chemical Sensor 22
  - Photo electrolysis production of Hydrogen 24
  - Photocatalytic degradation of organic pollutants 27
- Rhodamine B 27
  - Degradation of Rh B 27
- Spectrophotometer - beer-Lambert 31

Experimental 32
- Preparation and fabrication of TNTs 32
- Degradation of Rh B 33
- Nickel Deposition. 34
- Equipment 35
  - SEM 35
  - FESEM 35
  - Power supply 36
  - Eppendorf Spectrophotometer Operation 37

Results 38
  - SEM 38
  - FESEM 39
  - XRD 42

Spectrophotometer 42
Discussion 44
Catalyst Preparation 44
Catalyst characteristics 45
Morphology 45
XRD 45
Catalyst Activity 47
Future work 48
Conclusion 49
Bibliography 50
Appendix 52

List of Figures

Figure 1 Schematic set-up for anodization experiments [4] 12
Figure 2 A typical current density vs. time plot produced during the anodization process. [5] 13
Figure 3 Schematic representation of the Ti anodization (a) in absence of fluorides (results in flat layers), and (b) in presence of fluorides (results in the tube growth). [4] 14
Figure 4 Phase states TIO2 [6]. 16
Figure 5 Annealing Temperature [7]. 16
Figure 6 Cracks on TNTs surfaces. [7]. 17
Figure 7 Distribution of energy levels introduced into the bandgap [2]. 18
Figure 8 CdS RhB degradation Concentration [10]. 20
Figure 9 NiO/TNTs efficiencies [11] 20
Figure 10 TNTs array Solar Cell [2]. 21
Figure 11 Resistance of a 20 V sample when exposed to different concentrations of hydrogen at 290 1C. The nitrogen–hydrogen mixture was passed for 1500 s; the chamber was then flushed with nitrogen for 3000 s before passing the nitrogen–hydrogen mixture again [7]. 22
Figure 12 Plot of Current vs time of TATP detection, section A and C are absent of TATP vapours and SECTION C is in presence [7]. 23
Figure 13 Depiction of the Hydrogen production mechanism with TIO2 [14]. 25
Figure 14 calculated H2 generation rate related to Sensitization [10]. 26
Figure 15 Probable mechanism for the photocatalytic degradation of RhB dye [18]. 30
Figure 16 Photocatalytic Reactor 33
Figure 17 N1 Section A 110000x 38
Figure 18 N1 Section B 110000x 38
Figure 19 N1 SURFACE 910x 38
Figure 20 N1 Section B 110000x 38
Figure 21 S1 Surface 5500x 38
Figure 22 S1 Surface 910X 38
Figure 23 S11 Section A x100000 39
Figure 24 S11 Section B x100000 39
Figure 25 S11 Section C x100000 39
Figure 26 S11 Section D x100000 39
Figure 27 S12 Section A x100000 39
Figure 28 S12 Section B x100000 39
Figure 29 S12 section C x100000 40
Figure 30 S12 section D x100000 40
Figure 31 S13 Section B x100000 40
Figure 32 S13 Section B x100000 40
Figure 33 N11 Section A x100000 40
Figure 34 N11 Section B x100000 40
Figure 35 N11 Section C x100000 41
Figure 36 N12 Section A x100000 41
Figure 37 N12 Section B x100000 41
Figure 38 N13 Section A x100000 41
Figure 39 N13 Section B x100000 41
Figure 40 N13 Section C x100000 41
Figure 41 Graph showing XRD analysis, intensity vs 2 θ (degrees). 42
Figure 42 degradation of rhodamine B change Electrolyte 42
Figure 43 DEGRADATION OF RHODAMINE B CHANGE in Annealing Temperature 43

Figure 44 DEGRADATION OF RHODAMINE B With Sensitization 43
Figure 45 XRD pattern TIO2 Anatase (a) , Ritual (R) [20]. 46
Figure 46 Attendance form. 52

List of Tables

Table 1 Summary of physical properties of TNTs prepared under various conditions [6]. 15
Table 2 THE MOLECULAR STRUCTURE AND CHEMICAL PROPERTIES OF RHODAMINE B DYE. [17] 27
Table 3 Ethylene Glycol Based Electrolyte 32
Table 4 Glycerol Based Electrolyte 32
Table 5 Sample DEGRADATION EFFECENECY 47

Introduction.

The study of Carbon Nanotubes by Sumio Iijima in 1991 [1] showed that there was great potential in one-dimensional nanostructures. "one-dimensional (1D) nano-structures provide unique electronic properties, such as high electron mobility or quantum confinement effects, a very high specific surface area, and even show a very high mechanical strength" [2]. Sumios' research on One-dimensional nanostructures spurred wide interest in nano-scale technology, one-dimensional nanostructured metal oxides were found to support complex structures such as nanotubes, nano-rods and nano-wires. Titanium also became widely studied recently due to its profound mechanical properties such as high corrosion resistance and good bio-compatibility. Titanium oxides have also gained interest as it possesses interesting unique abilities such as the ability to self-cleaning and sense gas. [3] The properties of titanium oxide injunction with nanostructures gives mechanical functional properties that allow titanium dioxide nano-tubes to have solar energy and photo catalysis applications.

The primary role of this project thesis is to overview the synthesis methods of Titanium dioxide Nano-tubes and then to give insight into possible applications of the technology. The document tries to optimise factors of titanium dioxide nanotube fabrication and synthesis towards a photocatalytic application. Titanium dioxide works well as a photo catalyst by increasing the surface area of the Titanium dioxide through changing the structure of the titanium dioxide the photocatalytic effectiveness increases.

The use of Dyes has dramatically increased as they are greatly important in 21st century life, the uses of dyes ranges from manufacturing drugs to electronics, with the increase use there is also an increase in the waste products. Titanium dioxide nanotubes have shown that they have good photocatalytic properties and can effectively increase the photocatalytic degradation of dyes like Methyl blue and Rhodamine B. The test of this thesis will be conducted with a photocatalytic reactor containing Rhodamine B and titanium foil containing highly ordered titanium dioxide nanotube arrays, the concentrations of Rhodamine B will be graphed over time to help optimise the fabrication process of the titanium dioxide nanotube array as a photo catalyst.

Titanium dioxide nanotube arrays can be modified through many methods. The most common way of increasing and optimisation of the application of TNTs is achieved via lowering the band gap energy requirement to excite electrons from the valence band and conductance band and when illumination of the material is important increasing the spectrum of absorbance. The changing of these two characteristic material properties is done by changing the fabrication and synthesis process of the titanium dioxide nanotubes. The process of fabrication and synthesis can be changed by introducing elements by doping and sensitization. The introduction of doping species can greatly reduce the band gap energy requirement, sensitizing the material also has the same effect.

Literature review

Electrolysis

The fabrication of TNTs will be conducted by electrolysis, an understanding of the electrolysis process is relatively simple however is not taught in Mechanical engineering.

Electrolysis is the process of electrochemical anodization however electrolysis can be applied to other metals not just titanium, so the following process described will reference "M". The self- organized oxide tube arrays can be synthesised through this process. When a sufficient anodic voltage is applied in an electrochemical configuration (seen in figure below), an oxidation reaction occurs as follows $M \rightarrow M^{n+} + ne^-$ [2]. The electrochemical process occurs.

Oxidation of ions happens at the anode and reduction at the cathode for example oxidizing a metal.

EQUATION 1

$$anode\ M(aq) \rightarrow M^+(aq) + e^-$$

EQUATION 2

$$cathode\ MO + e^- \rightarrow MO^-$$

1. The electrolyte solution is saturated with M^+ ions.
2. M^+ ions react with O^{2-} ions and form an oxide layer on the metal which is often not soluble.
3. The Formation of Porous M oxide occurs and caused by competition from solvatization and oxidization.

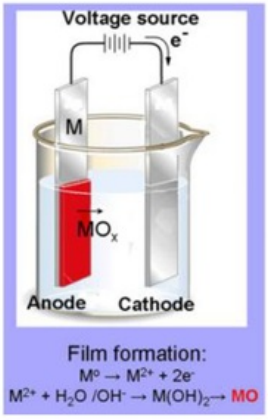

FIGURE 1 SCHEMATIC SET-UP FOR ANODIZATION EXPERIMENTS [4]

Titanium Dioxide Nanotube Arrays

Formation

The process of formation which was used in this thesis was through electrochemical anodization. The formation of metal oxides can be further controlled in electrolysis by the addition of an oxidation compound such as fluoride [4]. The addition of soluble fluoride causes a complexion between oxidation and metal oxide mineralizing process. The competition between anodic oxide formation and the chemical dissolution of the metal oxide can take place as soluble fluoride complexes the metal oxides into solution and follows the following reactions [4] [1].

EQUATION 3

$$Anodic\ oxide = Me + 2H_2O \rightarrow > MeO_2 + 4H^+ + 4e^-$$

EQUATION 4

$$\text{dissolution of the oxide as soluble fluoride complexes} = MeO_2 + 6F^- \rightarrow [MeF_6]^{2-}$$

EQUATION 5

$$\text{direct complexation} = Me^{4+} + 6F^- \rightarrow [MeF_6]^{2-}$$

The presences of fluoride ions cause for the formation of metal oxide nanotubes typically in three stages. The first is the initial barrier layer formation then pitting, formation of a porous surface or nano pore formation and then finally nanotube grow. [5]

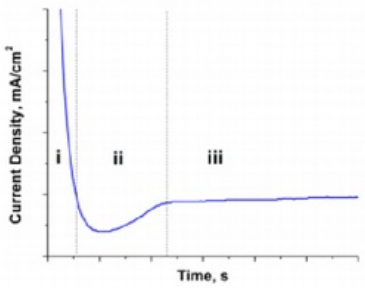

FIGURE 2 A TYPICAL CURRENT DENSITY VS. TIME PLOT PRODUCED DURING THE ANODIZATION PROCESS. [5]

The process is current self-limiting, as the formation of oxides occurs the resistance increases. The initial stage of barrier layer formation has a large current density as there is no or little oxide layer seen in the high current density in the figure above (stage i). The initial large current density indicates the applied anodic potential which causes the oxidation of Ti to Ti^{+4}. The current then rapidly decreases due to the formation of an oxide layer via the following hydrolysis reaction [5].

EQUATION 6

$$\mathrm{Ti^{4+}} + + 2H_2O \rightarrow \mathrm{TiO_2} + 4\mathrm{H^+}$$

As the reaction progresses H^+ ions accumulate on the surface and to maintain neutral state opposing F^- ions migrate from solution to positively charged H^+ sites. When a critical concentration of F^- ions is reached in local regions the dissolution of TiO_2 occurs by the formation of aqueous hexafluoro titanate

EQUATION 7

$$\mathrm{Ti^+} + 2\mathrm{H} + + 6\mathrm{F^-} \rightarrow \mathrm{H_2TiF_6}$$

This dissolution reaction causes negatively charged cation vacancies on the surface of the titanium which migrate to the interface between the metal and metal oxide faces this is a result of the positive potential gradient across the interface. The metal cation vacancies near the interface promote the $\mathrm{Ti} \rightarrow \mathrm{Ti}^{4+} + 4\mathrm{e}^-$. The Ti cations can then transfer to the next available vacancy. This promotion is results in a slight increase in current seen in the figure above (stage ii). During the dissolution and oxidation of Ti the nucleation of nanopores occurs at the surface of the metal. The balance of dissolution and oxidation allows for the continuation of current flow and the development of nanotubes. The balance of these two reactions causes constant current which is seen in the figure above (stage iii). This process can be modified by the changing of concentration of F^- ions which generally is caused by an increase of electrolyte concentration or voltage differential.

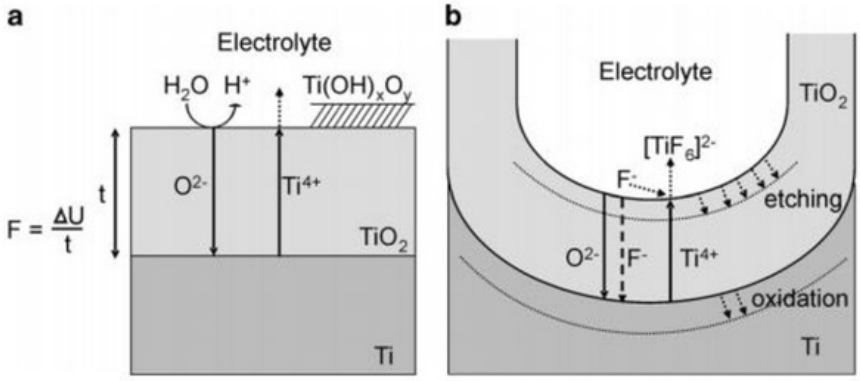

FIGURE 3 SCHEMATIC REPRESENTATION OF THE TI ANODIZATION (A) IN ABSENCE OF FLUORIDES (RESULTS IN FLAT LAYERS), AND (B) IN PRESENCE OF FLUORIDES (RESULTS IN THE TUBE GROWTH). [4]

Figure 3a depicts the development of a TiO_2 layer which is without the presents of fluoride ions. Figure 3b shows that when fluoride is added the field-aided ion transport (O^{2-} and Ti^{4+} $ions$) occurs. This gives further control to oxide growth (Note that fluoride ions are not the only means of providing an ion transport system, other ions like sulphide ions can achieve the same affect). In the presence of fluoride ions, the oxidisation process becomes more complex as shown schematically inFigure 3b this is due to, the field-aided ion transport and ability to form water-soluble $[TiF_6]^{2-}$ complexes, seen in Equation 6 [4].

This complex leads to a constant chemical attack (dissolution) of formed TiO_2 and prevents $Ti(OH)$ precipitation. Titanium in the form of Ti^{4+} ions arrive at the oxide interface and can be solvatized to $[TiF_6]^{2-}$. After some time, pores form and a tree-like growth takes place. The individual pores start interfering with each other, and start competing for the available current. . The pores equally share the available current, and a self-ordering system takes place when stable conditions are established [4], this process is also described by Poulomi Roy et.al "there is a continuous transition from a hexagonal porous to a tubular structure" [2]. The optimized conditions lead to a situation where nanotubes are formed.

Modification

The modification of the fabrication and synthesis process can be changed to optimise for certain applications. The process of modification can typically be achieved by changing of parameters in the electrolysis process, annealing, doping and sensitization.

Electrolysis

Changing the attributes in the electrolysis is the main way to change the structure and formation of the TNTs. The electrolyte used in the electrolysis process can affect factors such as nanotube growth rates, maximum tube length, nanotube wall thickness and the degree of order of the formation of the nanotubes. The changing of the voltage attributes such as changing the maximum voltage, current, and phases can have a profound effect on the tube structure. It is reported that electrolytes with an ethylene glycol base can achieve nanotube lengths of up to 1000nm [6]. By introducing a function to the voltage, particular structures such as double wall and bamboo nanostructures can be formed. The table below shows different attributes and resultant effect on diameter length and wall thickness.

TABLE 1 SUMMARY OF PHYSICAL PROPERTIES OF TNTS PREPARED UNDER VARIOUS CONDITIONS [6].

Length/μm	Thickness[a]/nm	Diameter/nm	Voltage/V	Time/h	Temp./°C	Main solvent	Conditions	Ref.
0.120	9	22	10	6	50	H_2O	0.5% HF + acetic acid (7:1)	23
0.156	13.5				35			
0.176	24				25			
0.224	34				5			
0.36	17	46	12		5	H_2O	0.5% HF + acetic acid (7:1)	24
0.5	<10	150	5–15	4	30	Glycerol	0.5 wt% NH_4F	25
0.5			5–15			Glycerol	0.5 wt% NH_4F	
3.5			60			EG	0.25 wt% NH_4F	
18			20–60			EG	0.25 wt% NH_4F	
0.5	15	100	20	2		H_2O	0.5 wt% NH_4F	26
2.5							1 M H_2SO_4/0.15 wt% HF	
1.9–5.7	8	30	20	16–70	RT	GL	0.5 wt% NH_4F	27
5	8	70	35	2	RT	EG	0.25 wt% NH_4F + 0.75 wt% H_2O	28
7	8		35	4				
14	8		35	20				
6	20	110				H_2O	0.1 M KF + 1 M $NaHSO_4$ 0.2 M trisodium citrate sodium hydroxide	29
6.5	20	110	25	17	22	H_2O	0.1 M KF + 1 M $NaHSO_4$ + 0.2 M trisodium citrate with sodium hydroxide	30
10		100	40	6		EG	0.25 wt% NH_4F	31
10	<20	15–110	20–50	1	RT	EG	0.25 wt% NH_4F 10 wt% H_2O	32
15			50	12		EG	0.25 wt% NH_4F	33
25				24				
40				48				
7–35	15	130	60			EG	0.25 wt% NH_4F, 2 vol% H_2O	34
134	25	160	60	17	20	EG	0.25 wt% NH_4F	35
45	15	120	40	69		DMSO	2% HF	
93	—	200	60	70		DMSO	2% HF	
70	24	180	35	48		Formamide	1–5 wt% H_2O, 0.3–0.6 wt% NH_4F	
220	50	110	50	17	20	Formamide	NH_4For HF, 2% H_2O	36
						DMSO		
						EG		
360	20	120	60	96	22	EG	0.3 wt% NH_4F, 2% H_2O	37
380				168			0.3 wt% NH_4F	
538				168			0.4 wt% NH_4F, 2.5% H_2O	
1000				216			0.3 wt% NH_4F, 3.5% H_2O	

[a] Wall thickness.

Annealing

TNTs have an amorphous nature which allows them to be annealed with the presence of oxygen. The phases which it can take are anatase and rutile. The phase change to rutile for Titanium dioxide starts at $350℃$ seen in the figure bellow.

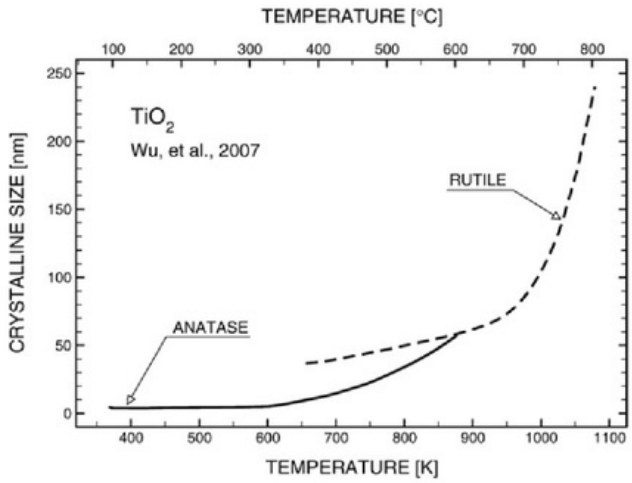

FIGURE 4 PHASE STATES TIO2 [6].

A higher purity of a state of either ritual or anatase shows an increase in photocatalytic and photochemical activity. In the study of "The preparation of highly ordered TiO2 nanotube arrays by an anodization method and their applications", Yongseok Jun et el found an increase of photocataltic activity in the production of methane using TNTs. The gradient delta in the annealing process at which the maximum temperature is reached at also affects the rutile and anatase phases. Heat gradients of $1℃s^{-1}$ s held at $900℃$ produced a structure completely comprised of a rutile structure [7]. The annealing process also provides an important function. Some electrolytes which use fluoride compounds to affect dissolution rates leave behind fluoride species, annealing drives out fluoride species formed in the electrolysis process which may have coated the titanium dioxide nanotube arrays.

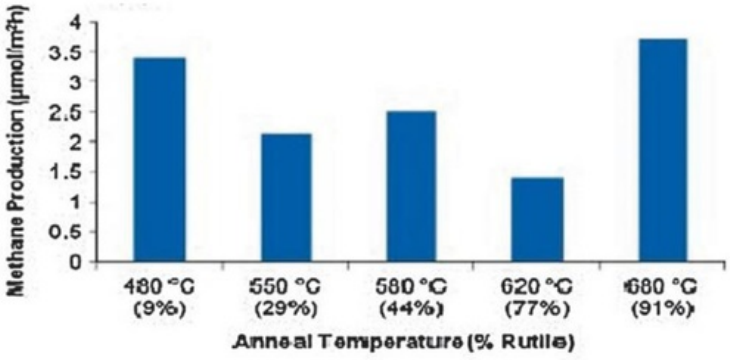

FIGURE 5 ANNEALING TEMPERATURE [7].

Annealing provides means to increase effectiveness in many applications however can also have unwanted affects in surface morphology. Annealing with temperatures above $450℃$ resulted in the formation of cracks. In higher temperatures above $650℃$ nanotube walls begin to collapse. [7].

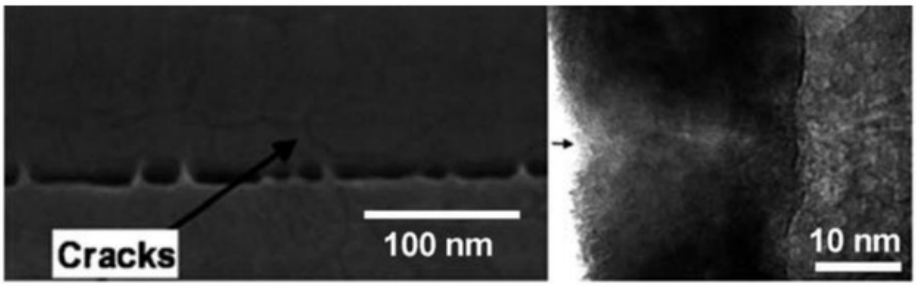

FIGURE 6 CRACKS ON TNTS SURFACES. [7].

Doping

Doping is a common practice in material science. The most important field of doping in technology would be the doping of semiconductors such as silicon. Doping of silicon allowed for specific functions such as changing the bandgap energy requirement. This of course lead to the replacement of the electronic valve for much smaller technologies as the transistors. The same principle of doping can be applied to TiO_2. In the last 10-15 years, great feats of engineering have gone into the introduction of secondary electronically active species into the TiO_2 lattice. The two drives for the doping of TNTs comes from the photocatalytic and photovoltaic applications. In both cases, doping is perused to exploit higher absorbance of electromagnetic spectrum and to reduce the band gap energy. Titanium Dioxide has an intrinsic band gap of 3.2 eV allowing for the material to absorb the ultraviolet range, meaning only 7% of the solar spectrum affectively absorbed, TNTs have a lower bandgap energy [7] caused by the structure. By doping material such as TiO_2 this band gap energy requirement can be decreased. The method of doping TNTs are as follows; treatment the final or developing TNTs with a solution or melted doping species, Thermal treatment or synthesis in a gaseous atmosphere with the doping species; producing the TNTs with methods of co-sputtering or sputtering in a gaseous atmosphere with the doping species.

The common method of doping TNTs is the hydrothermal or sol-gel process while the TNTs are being developed in electrolysis . The process is effective when the TNTs are in the range of nanometres. For Gaseous methods doping species such NH_3, CO and acetylene are used. The most successful and studied doping is nitrogen and carbon doping [8], however there is much debate and controversy around the use of nitrogen doping highlighted and it was advised that nitrogen doping should be avoided in experimental procedures. From the figure bellow the most active reduction of the bandgap are provided by nitrogen, carbon and sulphur. The reduction in bandgap of Nitrogen and carbon is around 0.5 E.v.

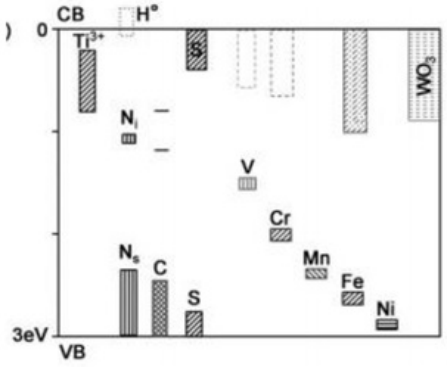

FIGURE 7 DISTRIBUTION OF ENERGY LEVELS INTRODUCED INTO THE BANDGAP [2].

Sensitization

Another method to achieve similar goals to doping is sensitization by filling, decoration and deposition. By introducing nanoparticles like other metals, semiconductors and polymers to the surface of the TiO_2 three possible beneficial effects can be achieved; heterojunction formation that changes band blending and can provide suitable energy levels for charge injection; catalytic effects for charge transfer reaction like the reaction of O_2 in photocatalytic particles and to have surface Plasmon effects which can lead to more efficient charge transfer. [2].

There are many syntheses such as chemical vapor deposition, electrochemical and wet-chemical techniques to obtain structures which are sensitized. In many solar applications, large band gap materials such as TiO_2 are sensitized with materials with smaller band gap ranges. This sensitization provides the same purpose as dye sensitized solar cells as sensitization allows injection of electrons excited by lower energy photons into the conductance band of large band gap semiconductors. The sensitization of larger band gap semiconductors have some advantages over dye sensitized solar cells as they have a specific quantum confinement effects as well as the ability to tune the particle size or composition to refine the absorbance of different wavelength of light, shown by Hodes [9]. Some of these semiconductor materials with narrow band gaps are CdS, PbS, $Bi_2S_3, CdSe, CdTe\ and\ InP$. Specifically, the sensitization of CdS was looked at by a fellow PhD student Yuxian Zhu. CdS was deposited onto TNTs and used as a photo catalyst to degrade Rhodamine B.

There has been considerate amount of work dedicated in investigating CdS as a sensitizer for TNTs. CdS sensitization on TNTs have approximate band gaps of 2.4 eV and coupled with a haigh absorption coefficient in the visible wavelength region which has made it desirable in photovoltaics and photo electrochemistry. CdS coupled with TNTs makes a suitable photoanode for solar energy conversion.

Cadmium Sulphide Sensitization.

Recently the interest of decorating TNTs with semiconductor quantum dots (QD) has greatly increased. QDs have a tuneable bandgap and large intrinsic dipole moments. This may cause an increase to visible light response and rapid charge separation. The out of the doping sensitizing materials mentioned previously; $CdS, CdSe, PbS, Wo_3\ and\ Cu_2o$, CdS has become the most studied material for decoration [10]. CdS show a narrow band gap and a relatively high absorbance range of solar light, thus making it very desirable in solar applications. Coupling CdS and Tio_2 and illuminating they are both simultaneously activated, this is owed to the synergistic effect. However, there is a formation of heterojunction where the contact interface can hamper election-hole recombination and causing a dominating charge separation. $CdS\ QDs$ have been reported to be decorated onto TNTs via electrochemical deposition and successive sonic layer absorption (SILAR), and sequential chemical bath deposition (S-CBD).

In the "Visable light induced photocatalysis on CdS quantum dots decorated TiO_2 nanotube arrays" by Yuxian Zhu et al, CdS where decorated onto TNTs and then used in a photocatalytic reactor to phototactically degrade Rhodamine B. $CdS\ QDs$ where decorated via the sequential SILAR method. TNTs where repeatedly dipped into a 0.1M solution of $Cd(NO_3)_2$ for 1 minute and then annealed for 12 hours at $80℃$ under vacuum. The report shows the after increasing the concentration of decorated CdS QDs on the TNTS via the repeated sequential SILAR method there was an increase in the photocatalytic effectiveness.

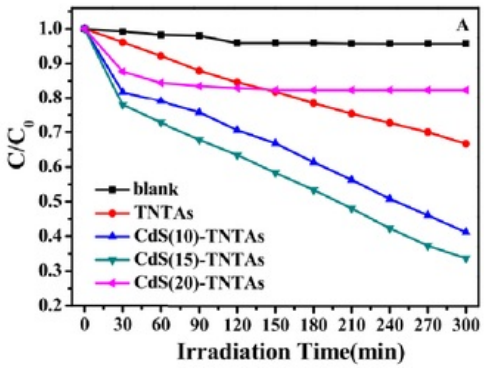

FIGURE 8 CDS RHB DEGRADATION CONCENTRATION [10].

The paper reports successfully increasing the photocatalytic activity, as seen from above increasing the CdS resulted in an increase in the photocatalytic effectiveness until the TNTs became over saturated and the photocatalytic performance became impeded.

NiO/N-doped TNTs.

Nitrogen doped materials have always attracted much attention from industry. The introduction of Nitrogen into TNTs has shown potential in reducing the energy band gap between the covalent band and valence band. In the "Construction stable NiO/N-doped TiO2 nanotubes photo catalyst with enhanced visible-light photocatalytic activity" by Huiong Li et al, the energy difference between the E_{CB} and E_{VB} bands was -0.16 and 2.78 eV [11]. The TNTs were produced by anodization in a glycerol (65vol%) H_2O electrolyte substrate containing 0.27 M NH_4F at 30V for 3 hours. The TNTs where annealed at $450℃$ for 3 hours to transform amorphous to highly crystalline anatase. The NiO loaded TNTs where achieved by soaking TNTs in ethanol contain 0.1M $Ni(NO_3)_2.6H_2O$ for 24 hours at room temperature and the further annealed at $300℃$ for 4 hours. Finally the NiO/TNTs were immersed in hydrazine for 6 hours and dried at $110℃$. The NiO/TNTs were used to degrade Rhodamine B and the degradation percent was found to be 60% [11] . Similarly to the CdS sensitization the NIO/N doped TNTs show an over concentration resulted in a reduction in effectiveness, seen in the figure bellow.

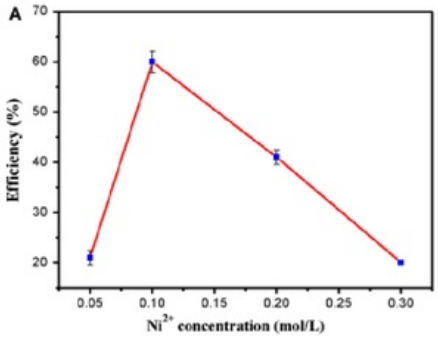

FIGURE 9 NIO/TNTS EFFICIENCIES [11] .

Applications

Photovoltaics

An attractive application is the use of TNTs in the use of solar cells. The dye sensitization of TiO_2 was investigate by Gerisher and Tributsch in 1968 [2] lead to the discovery of dye coated TNTs arrays in which TNTs acted as the photon-absorber layer of a solar cell, the schematic of the cell is shown in the figure bellow. The efficiency of the cell was about 11%, in comparison multi junction cells researched by UNSW have reached efficiencies of 34.5% [12] however this multijunction cell is comprised of different cells which have similar efficiencies.

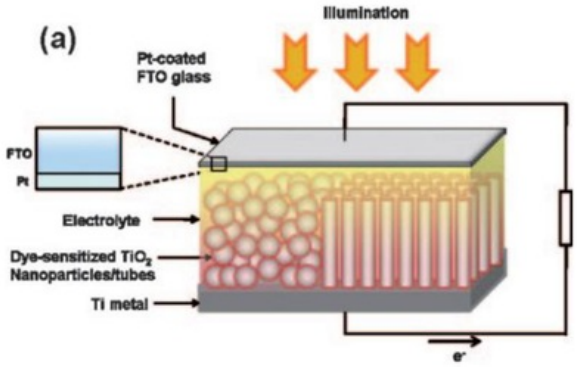

FIGURE 10 TNTS ARRAY SOLAR CELL [2].

The function of the cell works by the illumination of a dye which excites elections from the HOMO to the LUMO level, followed by rapid injection of excited elections into the conduction band of TiO_2. The elections flow to the back plate and then the oxidized dye on the surface is then regenerated by an electrolyte. It was found that nanotubes layers which where annealed in temperatures from $350℃$ to $450℃$ to form anatase tubes had greater efficiencies then those with rutile tubes. This is due to electron transport being fast in anatase crystal phases then rutile.

Chemical Sensor

Using titanium dioxide nanotube arrays as a chemical sensor has been explored recently, metal oxides have been used as chemical sensors as they are inexpensive, have simple working principle and high sensitivity. TiO_2 based gas sensors have become widely investigated as of high surface area property and high sensitivity. The working mechanism of chemical sensors originates from a surface phenomenon; nanostructures allow for advantages for chemical sensors as the structure can be designed for higher surface area to provide higher sensitivity.

A highly sensitive hydrogen gas sensor is critical for future hydrogen economies. Hydrogen has been considered for use in the automotive industry and is currently a greatly debated topic in greenhouse gas emissions. Highly ordered titanium dioxide nanotube arrays have been studied in hydrogen sensing due to their wide variation of electrical resistance in the presence of hydrogen [13].

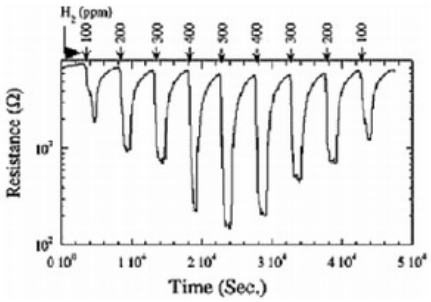

FIGURE 11 RESISTANCE OF A 20 V SAMPLE WHEN EXPOSED TO DIFFERENT CONCENTRATIONS OF HYDROGEN AT 290 1C. THE NITROGEN–HYDROGEN MIXTURE WAS PASSED FOR 1500 S; THE CHAMBER WAS THEN FLUSHED WITH NITROGEN FOR 3000 S BEFORE PASSING THE NITROGEN–HYDROGEN MIXTURE AGAIN [7].

The figure above shows a large resistance delta caused by the introduction of hydrogen gas onto a surface with titanium dioxide nanotube array. The range of resistance varies from $10^2\ ohms$ to $10^4\ ohms$. The increase in hydrogen results in a decrease of resistance. This resistance can then be digitised and used to analyse the content of hydrogen, this specific experiment was run at concentrations of 100 to 500 ppm in high purity nitrogen at high temperatures of $290\ ^{\circ}\mathrm{C}$. The principle of function is quite basic, electrons at absorbed H_2 and band blending induced by these charged molecules are responsible for the resistance change.

Recently TNT arrays have been used in counter terrorism applications. The most common homemade explosive used by terrorists is Triacetone Triperoxide (TATP). TATP comes in Dimer and Trimmer forms, TNT arrays can be used in aid to detect TATP. Zinc ions can interact with TATP, titanium dioxide nanotube arrays are exchanged with Zn^{2+} by using an aqueous solution of zinc sulphide ($ZnSO_4$). The process of surface hydroxyl proton exchange can be represented below [7].

$$2Ti - OH + ZN^{2+} \rightarrow 2Ti - OZn + 2H^{+}$$

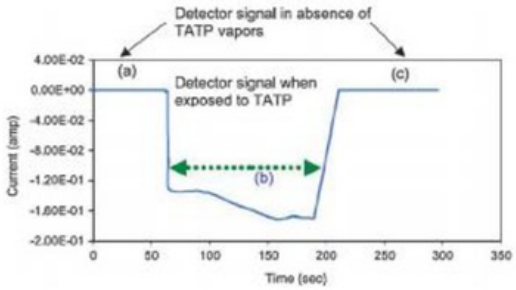

FIGURE 12 PLOT OF CURRENT VS TIME OF TATP DETECTION, SECTION A AND C ARE ABSENT OF TATP VAPOURS AND SECTION C IS IN PRESENCE [7].

The figure above shows that in the presence of TATP vapours the electrical current increases from 0 amps to $-1.7 * 10^{-1}\ amps$. This use of detection could be used to prevent terrorism as it provides a clear signal of detection of organic peroxide explosives.

Photo electrolysis production of Hydrogen

TNTs have been used to photocatalytic degrade organic compounds such as methyl blue and Rhodamine B, the photocatalytic properties of TNTs also extend into the production of hydrogen in photo electrolysis. The production of Hydrogen has become increasingly important as of the implications it has on the environment and global economy. The automotive industry is heavily dominated by fossil fuels which leave many pollutants after combustion. The combustion reaction of hydrogen is environmentally friendly; the reaction is as follows.

EQUATION 8

$$\text{combustion } 2H_2 + O_2 \rightarrow 2H_2O$$

The use of hydrogen is quite attractive as the product of the combustion reaction is just water meaning hydrogen powered vehicles have a much smaller footprint in comparison to fossil fuel vehicles which can leave behind led compounds, carbon monoxide and other pollutants. The drive for hydrogen fuel technology is greatly pursued by many car manufactures, TNTs have shown potential water splitting characteristics.

The use of a photo catalyst such as TNTs could mean a more cost effective solution in the production of hydrogen. The principle is to split water molecules into hydrogen and oxygen under illumination, ideally from direct sunlight. The sun is the biggest energy source in our solar system, almost every fuel that is used today could be argued to be powered from the sun given a large timeframe. All the fossil fuels are a result of the decomposition of plants which grew from photosynthesis. Solar technology allows for the direct harvesting of the suns energy. Currently solar to hydrogen energy conversion efficiency is too low for the technology to be economically viable. The two barriers to the use of photo catalysts to split water are the rapid recombination of phot-generated electron-hole pairs as well as the backward reaction and poor activation of TiO_2 in the relative application. Currently renewable energy contributes only about 5% of the commercial hydrogen production primarily via water electrolysis and while other 95% hydrogen is mainly derived from fossil fuels [14].

The mechanism for semiconductor photocatalytic hydrogen production occurs due to the excitement of the valence band and conductance band. When a semiconductor such as TiO_2 is excited by photons with equal or greater energy then the materials band gap energy level, electrons are excited by these photons and promoted from the valence band to the conductance band. For TiO_2 the follow reaction occurs:

EQUATION 9

$$TiO_2 + hv \rightarrow E^-_{TiO^2} + h^+_{TiO_2}$$

The process in the equation above can be represented by the figure bellow. The figure bellow shows the introduction of a photon to excite electrons in the TiO_2 valence band causing the separation of H_2 from a water molecule and simultaneously separating the reciprocal oxygen atom, on return another water molecule is split and releases another H_2 molecule and the two oxygen radicals form to make an O_2 molecule.

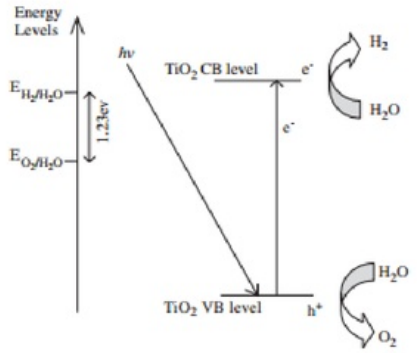

FIGURE 13 DEPICTION OF THE HYDROGEN PRODUCTION MECHANISM WITH TIO2 [14].

Photo-generated electrons and hole pairs can recombine in bulk or on a surface of a semiconductor in a very short time doing so releases energy in the form of heat or photons. The electrons and holes migrate to the surface of the semiconductor without recombination can reduce and oxidise the reactants absorbed by the semiconductor. The process of oxidization and reduction reactions are the basic mechanism of hydrogen productions. This process has several factors that affect the photocatalytic effectiveness in this application. The light source and quality of light is greatly important to the production of hydrogen if a fuel cell were to be comprised of a semiconductor such as TiO_2. The ability of TiO_2 to absorb the light is greatly important, as referred before TiO_2 only can absorb the UV spectrum which makes up 7% of the solar spectrum. To increase the absorption spectrum TiO_2 is often doped or decorated. Doping and decoration allows for the tuning of charge transfer between the electron-hole pair in the valence band and conductance however this doping and sensitization can affect the ion species and transfer on the surface of the material.

Water-splitting for hydrogen production using TiO_2 as a photo catalyst becomes challenging because of the rapid recombination of photo generated conductance band electrons and valence band holes. By adding electron donors to react irreversibly with photo generated conductance band electrons and valence band holes the photocatalytic electron-hole separation can be enhanced and result in higher quantum efficiencies. The introduction of organic compounds such as EDTA, methanol, ethanol and lactic acid the production of hydrogen can be increased, the effectiveness proceeds in that given order (EDTA being the highest) [14].

In "Visable light induced photocatalysis on CdS quantum dots decorated TiO_2 nanotube arrays" by Yuxian Zhu et al, CdS QDs where used to sensitize TNTs to observer the affect in the production of hydrogen. It was found that sensitizing TNTs to an extent resulted in high hydrogen production.

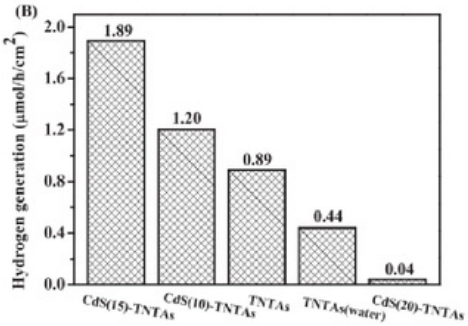

FIGURE 14 CALCULATED H2 GENERATION RATE RELATED TO SENSITIZATION [10].

The report shows that the sensitization increases the rate of hydrogen production by aiding in the photo generation process and states "To achieve higher photocatalytic efficiency, not only electron–hole pair should be generated by per photon in the visible light, but also the electrons and holes should be transferred to their respective reaction sites before their recombination. The following pathways could be occurred during hydrogen production on the catalysts" [10].

EQUATION 10

$$CdS/TiO_2 + hv \rightarrow CdS(h^+)/TiO_2\ (e^-)$$

EQUATION 11

$$TiO_2(2e^-) + 2H_2O \rightarrow H_2 + 2OH^-$$

EQUATION 12

$$2CdS(h^+) + SO_3^{2-} + 2OH- \rightarrow H2O + SO4\,2-$$

EQUATION 13

$$2CdS(h+) + 2S2^- \rightarrow S_2^{2-}$$

EQUATION 14

$$S_2^{2-} + SO_3^{2-} \rightarrow S_2O_3^{2-} + S_2^-$$

EQUATION 15

$$2CdS(h^+) + S_2^- + SO_3^{2-} \rightarrow S_2\,O_3^{2-}$$

The change in the hydrogen production mechanism by introducing CdS QDs was successful, the introduction of CdS QDs provided a mechanism to reduce electron-hole pare recombination and provided a wider absorbance range of the illuminated source.

Photocatalytic degradation of organic pollutants

The photovoltaic effect is a phenomenon where a voltage or electrical current ins induced in a material by being exposed to electromagnetic radiation, often and most commonly from the solar spectrum. This is the basis for semiconductor phot catalysis and photo electrochemistry. The first report of this phenomenon was by the French scientist Alexandre-Edmond Becquerel in 1839. [5]. Since this first advent the understanding of electrochemical interaction between semiconductor-liquid interfaces has greatly improved, namely by Gerischer, Memming and Williams [5].

The most photocatalytic active material for the decomposition of organic pollutants is Tio_2. The high activity for the photocatalytic degradation of organic pollutants is due to the band due position relative to the typical environment that the organic dye is situated in (Organic dyes are often situated in water). The basic principle is light promotes election from the valence band to the conduction band which results in the production of hydroxyl radicals.

Rhodamine B

Rhodamine B is an organic dye commonly used as an indicator in flow simulations, it is a synthetic green crystal or violet powder with the following chemical composition $C_{28}H_{31}ClN_2O_3$, Rhodamine B (Rh B) is highly soluble in water and alcohol with a bluish red fluorescence in solutions. [15]. The Rhodamine B is used extensively in biotechnological applications such as fluorescence microscopy, correlation spectroscopy and enzyme-linked immunosorbent assay.

Degradation of Rh B

The photocatalytic degradation of organic compounds such as Rhodamine B can be achieved via two means; direct hole oxidation or OH radical oxidation [16]. Titania photooxidation of organic pollutants can occur by both means of photocatalytic degradation [5]. Factors in determining the method and effectiveness of photocatalytic degradation are the position of the band gap edges and redox potentials of the pollutant. Photocatalytic degradation of pollutants in aqueous solutions typically occur due to interactions with reactive radical ions. When a pollutant is in an aqueous solution such as H_2O and being irradiated photo-charges react and form superperoxo $O_2^{\cdot-}$ and hydroxyl radicals $OH^{\cdot}$. Surface bound radicals interact with the organic pollutants (dye molecules) causes mineralization.

TABLE 2 THE MOLECULAR STRUCTURE AND CHEMICAL PROPERTIES OF RHODAMINE B DYE. [17]

Molecular structure	Chemical properties	
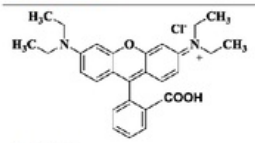	Chemical formula	$C_{28}H_{31}ClN_2O_3$
	Molecular weight	479.02 g/mol
	Absorption maximum	554 nm
Rhodamine B	Class	Triphenylmethane

Photocatalytic degradation or photooxidation occurs in direct charge transfer between TiO_2 and the organic pollutant. The position of the energy band gap of TiO_2 on the electrochemical potential scale allows it to be an effective photo catalyst, the position of the valence and conduction band become more important where it is thermodynamically favourable for charges generated by irradiation to be directly scavenged by the organic pollutant. The degradation reaction differs for different photosensitized oxidation reactions, the photo-process is initiated by visible light absorption of a sensitizer. Visible light excitation of the sensitizer leads to electron injection from the excited molecule into the conductance band of the TiO_2. The catatonic dye radicals generated from this process are as follows [5].

EQUATION 16

$$Dye + hv \rightarrow Dye^*$$

EQUATION 17

$$Dye^* + TiO_2 \rightarrow Dye^{\cdot+} + TiO_2(e^-_{CB})$$

EQUATION 18

$$TiO_2(e^-_{CB}) + O_2 \rightarrow O^{\cdot-} + TiO_2$$

EQUATION 19

$$Dye^{\cdot+} \rightarrow degradation\ process$$

The $Dye^{\cdot+}$ radicals can then be mineralized through reactions with hydroxyl ($OH^{\cdot}$) Radicals or interact with peroxo compounds ($O_2^{\cdot-}$,$HO_2^{\cdot}$ $OH^{\cdot-}$).

EQUATION 20

$$Dye^{\cdot+} + OH^- \rightarrow Dye + HO^{\cdot}$$

EQUATION 21

$$Dye + 2HO^{\cdot} \rightarrow H_2O + oxidation\ products$$

EQUATION 22

$$O_2^{\cdot-} + H^{\cdot} \rightarrow HO_2^{\cdot}$$

EQUATION 23

$$HO_2^{\cdot} + H^+ + TiO_2(e^-_{cb}) \rightarrow H_2O_2 + TiO_2$$

EQUATION 24

$$H_2O_2 + TiO_2(e^-_{cb}) \rightarrow HO^{\cdot} + HO^- + TiO_2$$

EQUATION 25

$$Dye^{\cdot+} + O^{\cdot-} \rightarrow DO_2 + degradation\ products$$

EQUATION 26

$$Dye^{\cdot+} + HO_2^-(or\ HO^{\cdot}) \rightarrow degradation\ products$$

Thillai Sivakumar Natarajan et al in the "Study on UV-LED/TiO2 process for degradation of Rhodamine B dye" provide a proposed mechanism for the degradation of Rhodamine B and its intermediary products. The study of Rhodamine B degradation path way under UV-LED light irradiation and to identify intermediate products formed in the degradation process electro spray ionization mass spectra (ESI-MS) experiments were conducted. "During the Electrospray ionization analysis, there was formation of several aromatic intermediate. The photocatalytic degradation of RhB by the photo generated active species such as •OH and hole could attack the central carbon of RhB to decolorize the dye and further degraded via N-de-ethylation process." [18]. The process of N-de-ethylation was taken place in the formation of nitrogen centred radicals during the destruction of the Rhodamine B chromophore structure. The degradation process of Rhodamine B caused by the photo generated hydroxyls ($\cdot OH^-$) to attack the central carbon of the Rhodamine B causing the decolourisation o the molecule. The figure below shows the N-de-ethylation process and mineralization into CO_2, H_2O, NO_3^- and NH_4^+.

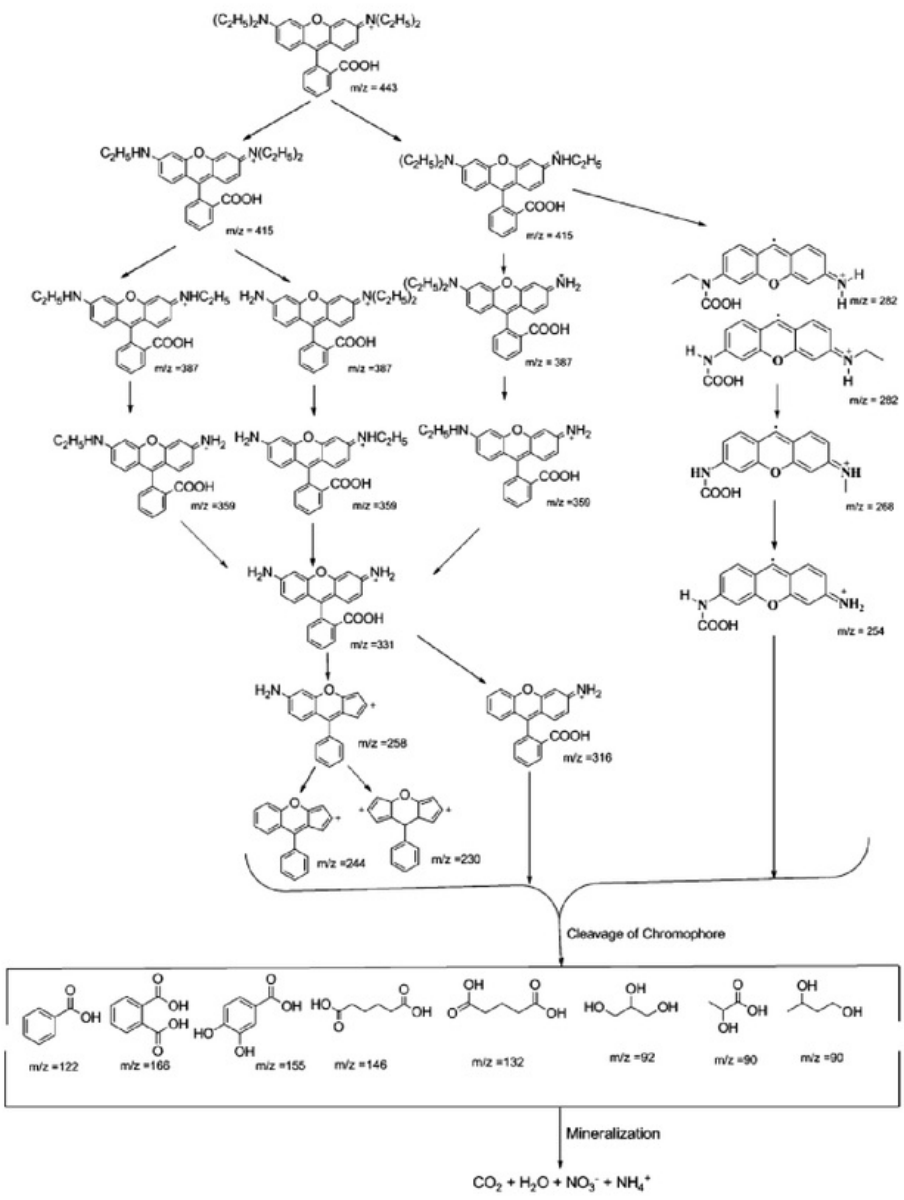

FIGURE 15 PROBABLE MECHANISM FOR THE PHOTOCATALYTIC DEGRADATION OF RHB DYE [18].

Spectrophotometer - beer-Lambert

To understand how to use the spectrophotometer some background knowledge was required. The beer-Lambert law was discovered by Pierre Bouguer in 1729, [Pierre Bouguer, Essai d'optique sur la gradation de la lumière (Paris, France: Claude Jombert, 1729) pp. 16–22]. The law relates the absorbance of electromagnetic radiation to the properties of a material through which the electromagnetic radiation is being emitted though. The law is often used for chemical analysis measurements to define attributes of a specific material. The law equates the transmittance of a material the depth of a material to absorbance. The transmittance of a sample is related to radiant flux is transmitted by a material, to the radiant flux received by the material and absorbance.

EQUATION 27

$$T = \frac{I}{I_0} = 10^{-A}$$

where T is transmittance, I_0 is initial radiant flux, I is the radiant flux received and A is the absorbance [19]. By changing this and manipulating the previous equation and defining relations through material properties; K, b and c we can use the following equation to derive concentration of a sample [19].

EQUATION 28

$$A = \log\left(\frac{1}{T}\right) = Kbc$$

Where K is the material constant *b* is the material width and c the concentration. The following proof shows that we can substitute the Absorbance (A) can be substituted for (C) when comparing a concentration with a subsequent concentration.

EQUATION 29

$$A = Kbc$$

$$let\ x = Kb\ as\ Kb\ are\ constance\ given\ the\ material\ matrix\ and\ width\ are\ constant$$

EQUATION 30

$$Ax = cx$$

$$Let\ n\ denote\ a\ sequence\ in\ a\ series\ A_n x = xc_n$$

EQUATION 31

$$A_{n+1}x = xc_{n+1}$$

EQUATION 32

$$\frac{A_n x}{A_{n+1}x} = \frac{xc_n}{xc_{n+1}}$$

EQUATION 33

$$\frac{A_n}{A_{n+1}} = \frac{c_n}{c_{n+1}}$$

Experimental

There was a high level of safety required as the process of fabrication, preparation and testing used hazardous chemicals such as Nitric acid and acetone. Work place safety was paramount and respective documentation such as SDS sheets and laboratory training was required, persona safety equipment such as safety goggles, latex gloves, lab coats and fume hoods were utilised.

Preparation and fabrication of TNTs

The method of Titanium dioxide nanotube arrays (TNTAs) fabrication was achieved by wet-chemical sol-gel electrolytic anodization using Ethylene Glycol (EG), Glycerol and water mixtures. The original method of synthesis was shown and conducted by PhD student Yuxiang Zhu over the progress of the thesis the method was adapted and changed to suit current equipment and material availability. The pre-treatment of titanium foil is very important in the formation of TNTS arrays, any surface impurities and oxides that may exist can cause unwanted artefacts after the electrolysis process. 50 mL of a nitric acid is prepared by diluting 95% nitric acid into water ($HNO_3{:}H_2O,\ 4{:}5\ V/V$). Titanium foil with a thickness of .5mm is cut into several sample sizes of 5cm by 2cm and placed in a nitric acid bath for ten minutes. The foil was then removed, washed with deionised water and ultrasonically bathed in acetone, methanol, ethanol and deionised water for ten minute intervals and washed with deionised respectively.

The sol-gel electrolyte used to synthesis the TNTs arrays was varied through the process and tested until optimised. The two sol-gel solutions used where; ethanol glycol and water and Glycerol and water. The two electrolyte groups where based on the two sol-gel solutions mixed with varying concentrations of ammonium fluoride. Ammonium fluoride in this electrolyte will be the provider of fluoride ions to allow dissolution of the TiO_2 to encourage the transition of porous TiO_2 to organised TiO_2 nanotubes. The ammonium fluoride concentrations were varied from 0.2, 0.5, 0.7 and 1 wt%. There varying concentrations and weights are in the following indexing tables. Each sample was annealed at $450℃$ unless stated otherwise.

TABLE 3 ETHYLENE GLYCOL BASED ELECTROLYTE

Sample	Ethylene Glycol (mol)	Water (mol)	Ammonium Fluoride (mol)
S11	0.894	0.163	0.0337
S12	0.894	0.163	0.0111
S13	0.894	0.163	0.00793

TABLE 4 GLYCEROL BASED ELECTROLYTE

Sample	Glycerol (mol)	Water (mol)	Ammonium Fluoride (mol)
N11	0.339	1.39	0.00304
N12	0.339	1.39	0.00763
N13	0.339	1.39	0.0107

The cleaned Ti foils are then used as an anode and a platinum electrode was used for the cathode. The power supply used for electrolysis was the PST-3302 programmable power, the programable power supply was controlled via the coding language python and a voltage step of 250mV/s was used. The titanium foil was attached to the anode and the face pointing to the cathode was noted, this is the side with the TNTs growth. Once 20V was reached the electrolysis was conducted for 2 hours. The TNTs foils where then removed and were ultrasonically bathed in distilled water for 1 minute. The step of bathing the TNTs foil is needed to remove any residual electrolyte. The TNTs foils where then annealed with the TNTs face up for 3 hours at $450℃$ with a $2℃/s$ heat gradient.

Degradation of Rh B

Rhodamine B is needed to diluted into solutions to allow for ion transfer between the photo catalyst, it can be diluted into water, ethanol and other organic compounds. The most suitable case for Rhodamine B dilution is in distilled water to mimic real world applications like fluid dynamic analysis. A flask is filled with 1L of deionised water and 5 milligrams of Rhodamine B 95% was mixed into the solution. The solution was mixed vigorously for several minutes and underwent ultrasonication for 10 minutes.

The photocatalytic reactor was comprised of a condenser and a 300W Xeon lamp. 25Ml of 5mg/L Rhodamine B was decanted into a 50-ml beaker, a 1 cm by 2 cm TNTs foil was cut and held in an incision made on a Q-tip, the foil was suspended 1 cm down from the surface with the TNTs faced upwards in a 50-ml beaker and placed 13 cm under the Xeon lamp and in a water-cooled condenser which was situated on stir pad. A 1ml sample using was taken an Eppendorf spectrophotometer and then replaced every 10 minutes for 2 hours. The 300W Xeon lamp was operated at 10 amps. See the figure bellow for the photocatalytic reactor schematic.

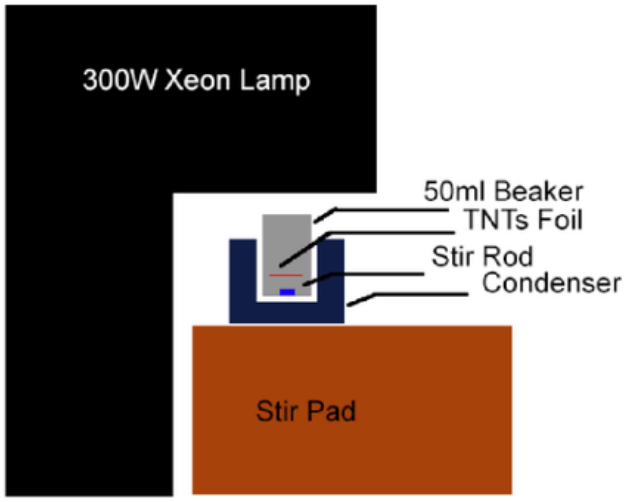

FIGURE 16 PHOTOCATALYTIC REACTOR

Nickel Deposition.

There were two methods of deposition as the first method produced unsuspected results and was very time expensive to develop this means of deposition however it will be discussed. The first method of deposition required the use of Sodium borohydride and Nickel nitrate hexahydrate and the method which was employed involved the decomposition of Nickel nitrate hexahydrate with the use of the Xeon lamp used in the degradation process.

The original method of deposition Sodium borohydride used H_2O based on a method designed by fellow students Yuxiang Zhu and Xujun Zhang. "Firstly, to synthesize Ni/C_3N_4 NTs with molecular weight of 1%, 1 gram of as-prepared g-C_3N_4 NTs is dispersed in 200mL of cool deionized water. The mixture is then stir in ice water for one hour, followed by 48 seconds of ultrasonic treatment. Afterwards, 0.0496 gram of nickel nitrate $Ni(NO_3)_2$ is then dispersed in the mixture which is stir in ice water for another 30 minutes. After stirring, the mixture is allowed for 10 seconds of ultrasonic treatment. At the meantime, 0.9458 gram of sodium borohydride $NaBH_4$ is dispersed in 25mL of cool deionized water and 2.73mL of reaction mixture is extracted and added to the previous mixture and stir for another 1 hour. After stirring, the mixture is placed in the normal environment for 1.5 hours. The particles of the mixture are then separated by a centrifugate, followed by one time of washing by deionized water and three times of washing by ethanol. The product is a combination of required photo catalyst and moisture, which will become pure photo catalyst Ni/C_3N_4 NTs with 1% after one night in a vacuum oven at 80°C." - Xujun Zhang

EQUATION 34

$$Ni(NO_3)_2 + 2NaBH_4 + 6H_2O \rightarrow Ni + 7H_2 + 2NaNO_3 + 3H_3BO_3$$

The method of using just water was modified to use ethanol and water mixture so encourage the coating of $Ni(NO_3)_2$ on the TiO_2 surface. This method was derived using hydroxyls similar in the last equation as the $Ni(NO_3)_2$ would form in a mixture solution of C_2H_6O and H_2O, from the previous equation the following hydroxyls would be formed and interchanged with similar species from of C_2H_6O. C_2H_6O *can be writen as* C_2H_5OH to help emphasise ion transfer.

EQUATION 35

$$H_2O \rightarrow H^+ + OH^-$$

EQUATION 36

$$C_2H_6O \rightarrow C_2H_5^+ + OH^-$$

Hydroxyls from the Nickel Nitrate Hexahydrate contains the H_2O so the addition of ethanol, through entropy could form with ethanol ion species and the following chemical equation occurs.

EQUATION 37

$$Ni(NO_3)_2 + 2NaBH_4 + 6C_2H_5OH \rightarrow Ni + 7H_2 + 2NaNO_3 + 2B(C_2H_5O)_3$$

TNTs foils where submersed in a 50Ml solution of an ethanol water mixture (C_6H_5O: H_2O, containing; 1 mM, 5mM and 10mM of Nickel nitrate hexahydrate for 12 hours and then placed under a 300W Xeon lamp for 2 hours. After being treated under the Xeon lamp the samples where then heated for a further 12 hours at 80℃ in a vacuum oven. The samples where then tested for the degradation of Rhodamine B.

Equipment

SEM

The nature of this project requires a structural view on the TNTs to look at the morphology of the tubes to see if the fabrication method is adequate to produce nanotube walls which are uniform. To obtain this information a scanning electron microscope SEM machine was used. The first tests and use of a SEM machine was the Phantom Desktop SEM machine which was made available via a sales instruction and pitch event held by Dr William Lawler. The desktop SEM allowed for quick access and overall images in the early weeks of the project which helped develop the synthesis process. The first SEM images provided enough resolution at 100K magnification to identify there was an issue with the fabrication of the TNTs. It was evident that there was residue electrolyte on the surface from the fabrication process.

FESEM

The Pictures which were taken with the Phantom Desktop SEM were suffice enough for basic information to be drawn. The requirement for higher quality pictures was needed and the access to the Phantom Desktop SEM had a limited timeframe. The solution to get higher picture quality was use of a FESEM machine which was in the Macquarie university microscopy lab. The picture quality which was obtained from the FESEM are of much higher quality and resolution however the training and operation of the FESEM is very costly and time consuming.

Since the FESEM is operating at such high magnification (of up to 1 million times) focusing the image becomes very sensitive to factors such as stigmation, alignment and electromagnetic interference. The understanding of stigmation was required to get high quality pictures for this project. Stigmation occurs when the electron beam emitted is not focused on the sample properly. The beam must be aligned in both X and Y directions. By changing the beam stigmation the image no longer skews and the object can then be focused on.

The TNTs samples where cut into 1 mm by 1 mm squares and held on to black carbon tape and placed into a special holder. The holder was then inserted into the machine. Stigmation and alignment was acquired by changing the X and Y focus on various magnification levels. The FESEM operation voltage was increased to 15KV and 20KV to produce clearer pictures.

Power supply

The power supply used in the electrolysis was the PST-3302 programmable power supply. The programmable power supply was sourced from Mr Yimin Xie. Mr Yimin Xie provided an code which implements a VISA linking API developed by Key sight instruments, the code was heavily modified and compiled using Visual studio 2015. The following code was written in python and wraps PPS.exe to create a time-based voltage function, it reads from a comma separated values file (CSV) which has a specified voltage and current at a given time.

The initial voltage applied is a strong factor in developing the initial TNTs pores. With the pores being defined by the initial voltage ramping it is important to have specific and defined control over the voltage ramping. Voltage ramping refers to the rate at which the voltage is increased at. In the first weeks, in of the project the voltage was manually ramped by hand, changing the power supplied by rotating the dial on the power supply.

Code snippet:

```
import subprocess
import csv
from time import strftime, gmtime, time
import time

#reading voltage program
with open('voltageSeries.csv', 'r') as f:
        reader = csv.reader(f)
        VoltageProgram = list(reader)

initialTime = time.time()
progCounter = 1;
lastVoltage = 0;
subprocess.call(['PPSU.exe', 'on'])

# set opperation loop
while True:
    #compare time frame
    if time.time()-initialTime <= float(VoltageProgram[-2][2]):
        if float(VoltageProgram[progCounter][2]) >= time.time()-initialTime:
            if lastvoltage != VoltageProgram[progCounter][0]:
                # calling the PSU controller with voltage variables
                subprocess.call(['PPSU.exe', 'ch2', VoltageProgram[progCounter][0], VoltageProgram[progCounter][1], '32'])
                # printing virables and execution time
                print('PPSU.exe', 'ch1', VoltageProgram[progCounter][0], VoltageProgram[progCounter][1],
                        VoltageProgram[progCounter][2], time.strftime("%a, %d %b %Y %I:%M:%S %p %Z", time.localtime()))
                lastVoltage = VoltageProgram[progCounter][0]
            time.sleep(float(voltageProgram[progCounter][2])-float(voltageProgram[progCounter-1][2])-.001)
        else:
            progCounter += 1
    else:
        #breaking the program
        subprocess.call(['PPSU.exe', 'off'])
        break
exit()
```

Eppendorf Spectrophotometer Operation

The equipment used to measure the absorbance of the Rhodamine B was the Kinetic spectrophotometer by Eppendorf. The equipment was borrowed from Mark Tran in the chemistry department. The spectrophotometer is very sensitive to any changes in operation so the operation process was refined. Originally the corvette was cleaned with Deionised water and detergent and dried using Kemtec wipes, however the wipes left micro fibres on the quart's cuvette surface to avoid fibres affecting the absorbance measurements.

The microfibers residue from Kemtec wipes where causing a deviation of 0.05^{+}_{-} absolute absorbance readings. Nitrogen gas was used in drying process and three samples were taken and averaged at each sample interval and the orientation of the cuvette was noted, this was successful at making the results more valid as deviation was brought down to 0.0005^{+}_{-}.

The process was refined several times originally a sample of .2 ml was taken as a sample and diluted in 4ml of deionised water and tested, doing this resulted in concentrations which were too small for the Eppendorf machine to register so the amount of the dilatant was reduced to 2 ml and then 1.5ml of deionised water. The sample was taken 3 times and averaged, the sample size was also then changed to 1ml with no dilution process and was replaced into the rhodamine B solution in succession to the sample. This was originally avoided as it was thought it would interfere with succession samples however it was found to have no affect and allowed for concentration levels which could produces accurate and reliable results.

To get the level of concentration the beer-lambert law needs to applied. Noting that the more the Rhodamine B degrades to Rhodamine the absorbance decreases and by the proof previously extrapolated we can substitute $A/A0$ for $C/C0$ to get the degradation amount.

Results

SEM

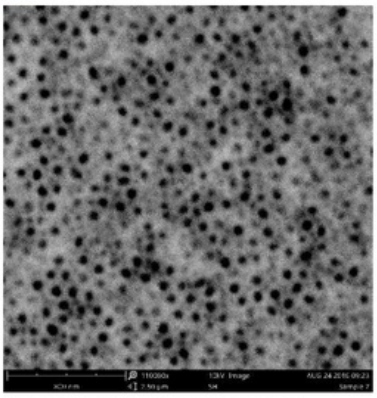

FIGURE 17 N1 SECTION A 110000X

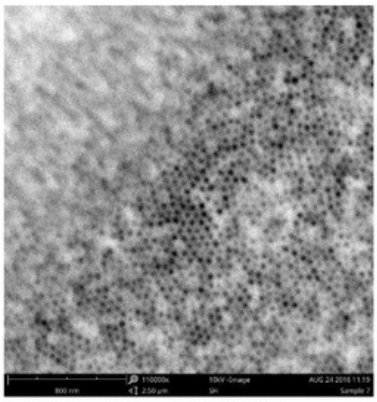

FIGURE 18 N1 SECTION B 110000X

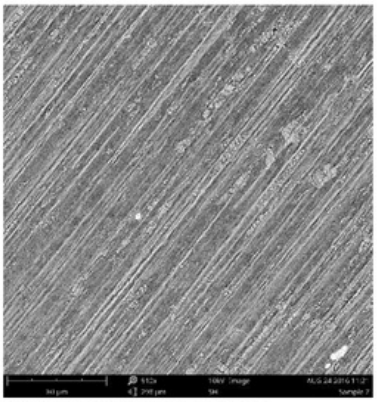

FIGURE 19 N1 SURFACE 910X

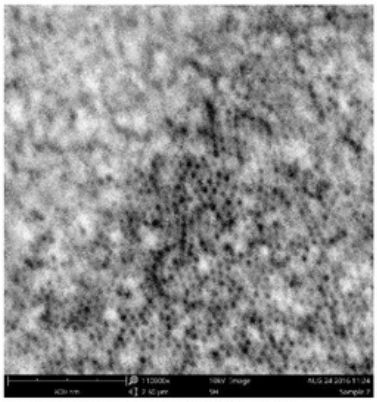

FIGURE 20 N1 SECTION B 110000X

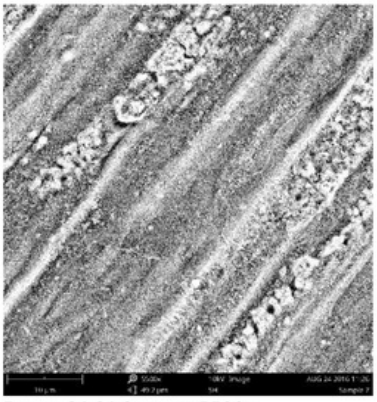

FIGURE 21 S1 SURFACE 5500X

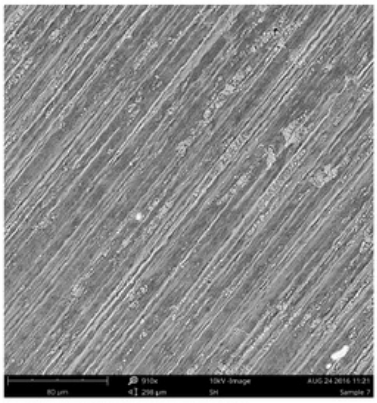

FIGURE 22 S1 SURFACE 910X

FESEM

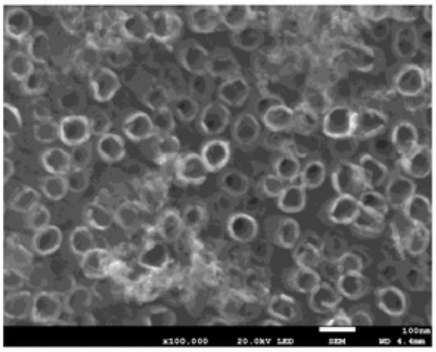

FIGURE 23 S11 SECTION A X100000

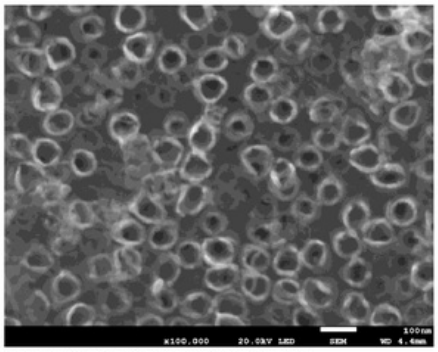

FIGURE 24 S11 SECTION B X100000

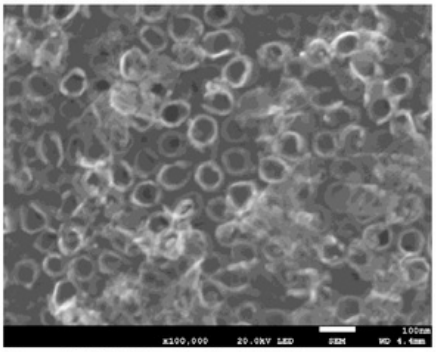

FIGURE 25 S11 SECTION C X100000

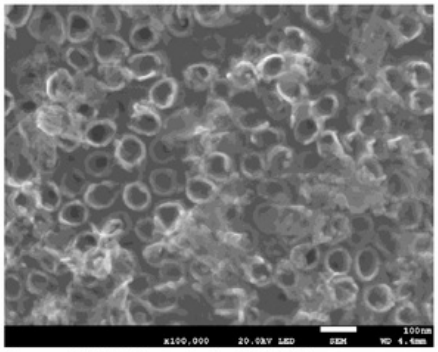

FIGURE 26 S11 SECTION D X100000

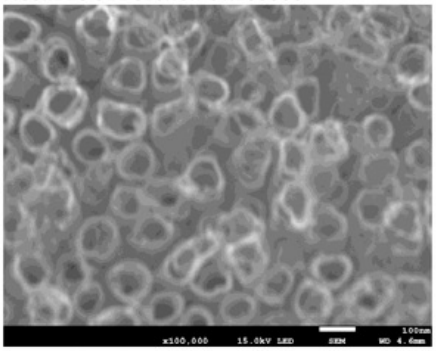

FIGURE 27 S12 SECTION A X100000

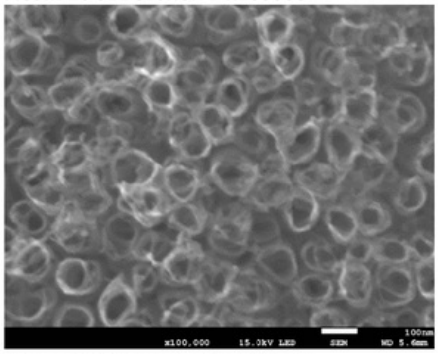

FIGURE 28 S12 SECTION B X100000

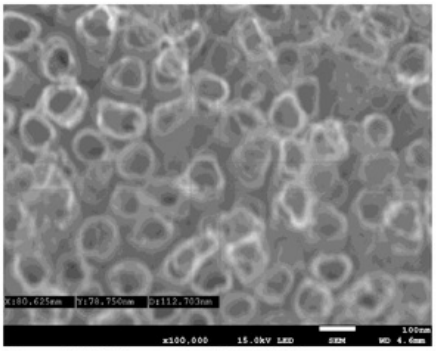

FIGURE 29 S12 SECTION C X100000

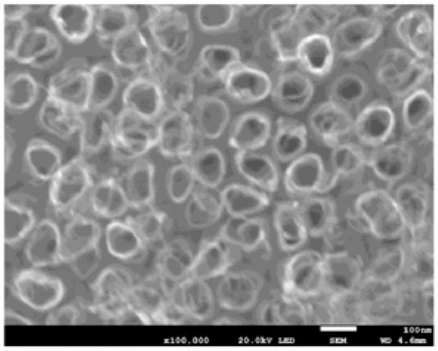

FIGURE 30 S12 SECTION D X100000

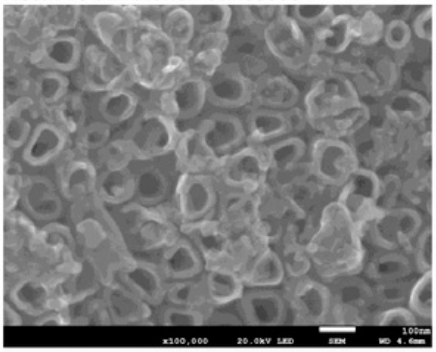

FIGURE 31 S13 SECTION B X100000

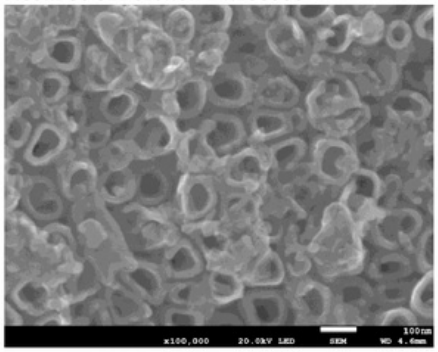

FIGURE 32 S13 SECTION B X100000

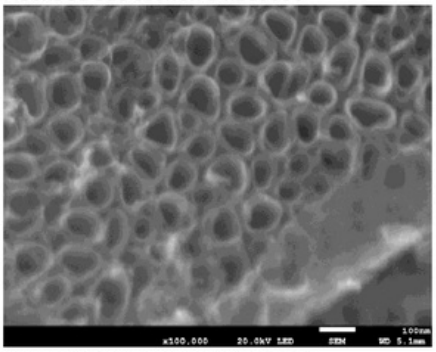

FIGURE 33 N11 SECTION A X100000

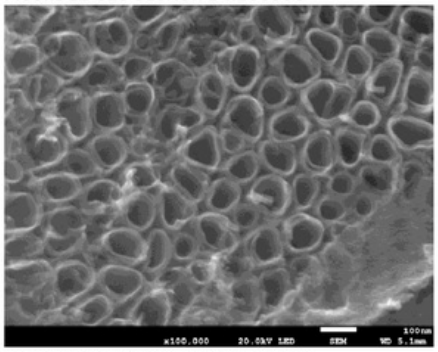

FIGURE 34 N11 SECTION B X100000

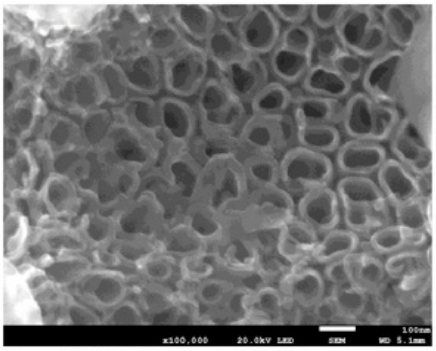

FIGURE 35 N11 SECTION C X100000

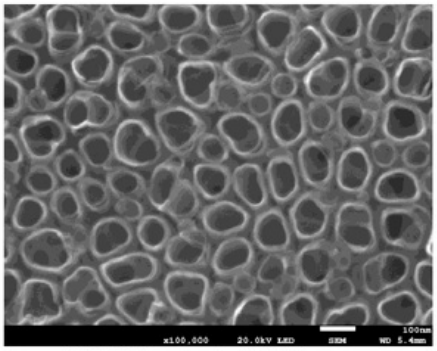

FIGURE 36 N12 SECTION A X100000

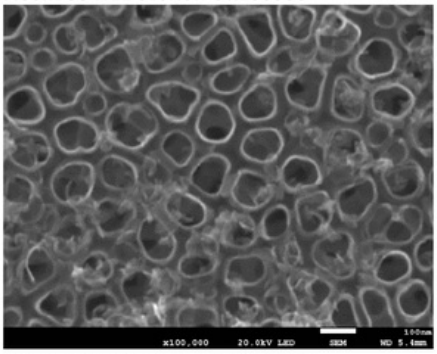

FIGURE 37 N12 SECTION B X100000

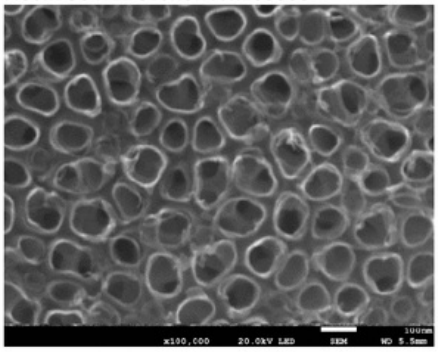

FIGURE 38 N13 SECTION A X100000

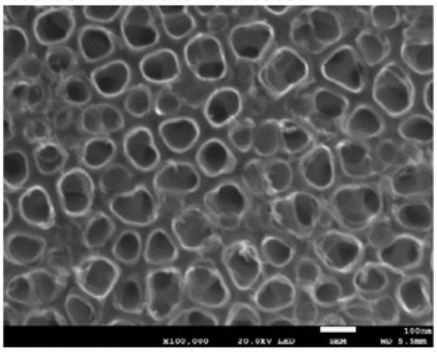

FIGURE 39 N13 SECTION B X100000

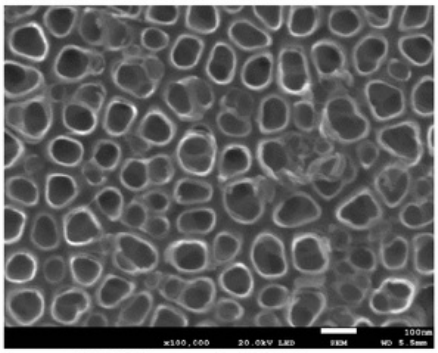

FIGURE 40 N13 SECTION C X100000

XRD

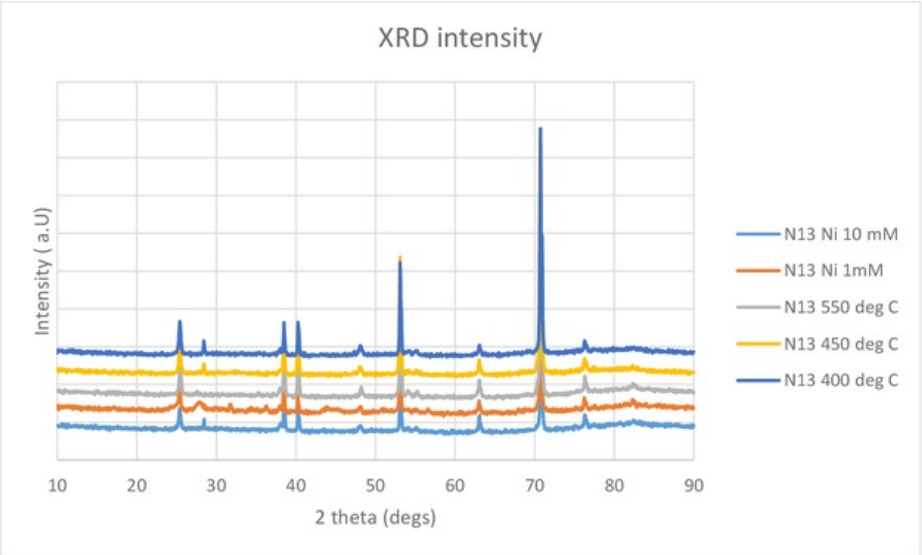

FIGURE 41 GRAPH SHOWING XRD ANALYSIS, INTENSITY VS 2 Θ (DEGREES).

Spectrophotometer

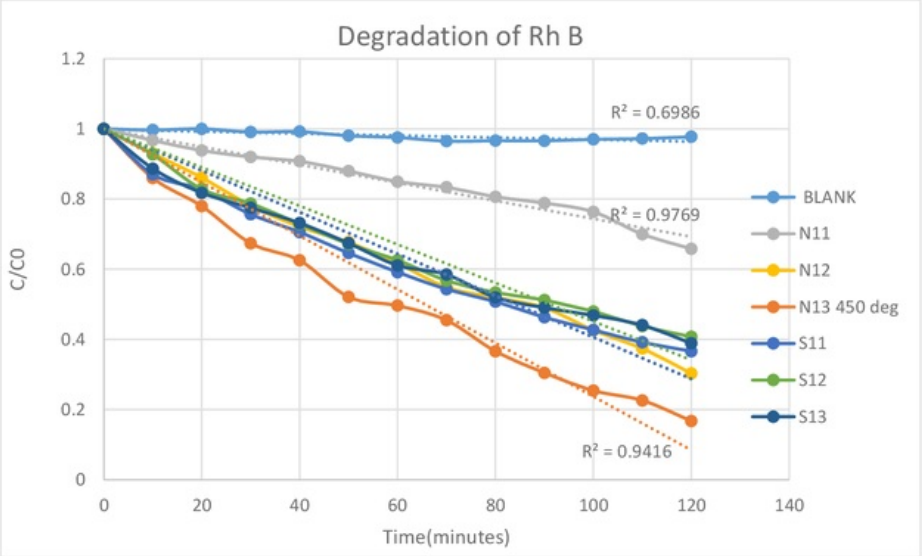

FIGURE 42 DEGRADATION OF RHODAMINE B CHANGE ELECTROLYTE

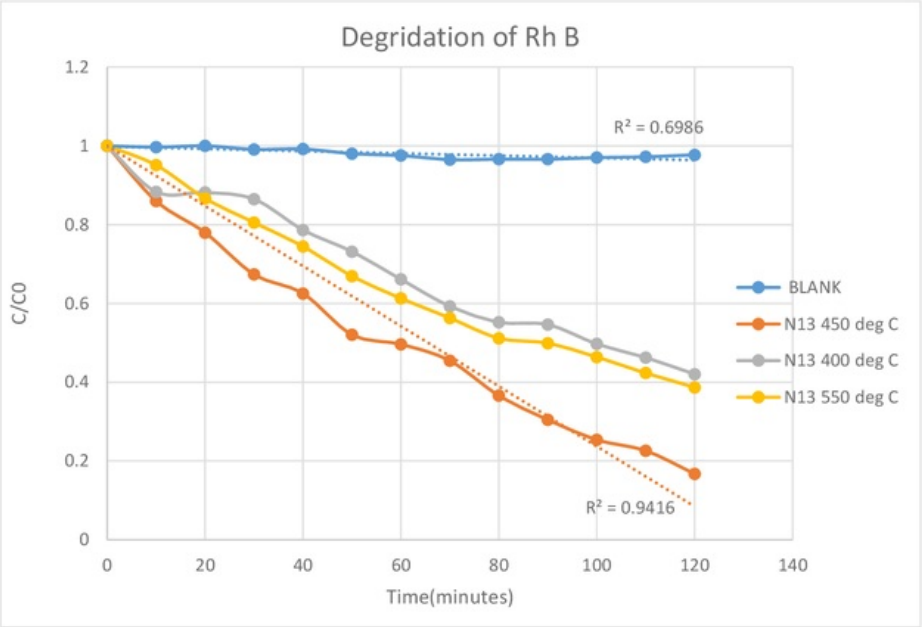

FIGURE 43 DEGRADATION OF RHODAMINE B CHANGE IN ANNEALING TEMPERATURE

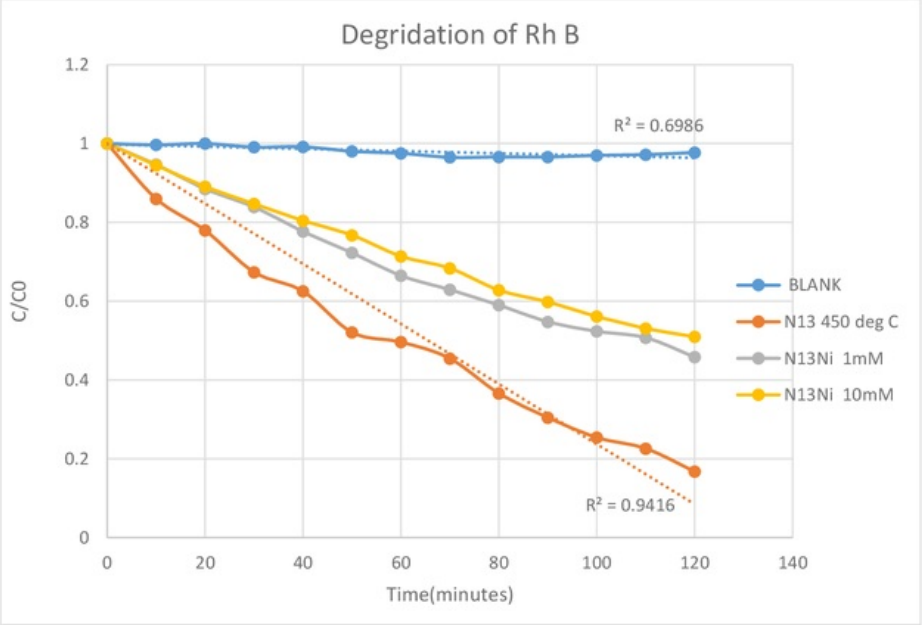

FIGURE 44 DEGRADATION OF RHODAMINE B WITH SENSITIZATION

Discussion

Catalyst Preparation

The pictures taken with the Phantom Desktop SEM machine provided information which lead to changing and optimisation of the fabrication process. Figure 17 N1 Section A 110000x showed that there were artefacts on the surface of the TNTs foil. A portion of the pores from the SEM imagery where closed and coated by the electrolyte left from the electrolysis process. The surface of the titanium foil showed micro scratches seen in the granular patterns on Figures 17 and 20. The surface of the foil appears to be very rough and coarse at magnifications of approximately 1000 times. There was an inclusion of a step in the fabrication process where the TNTs foil was ultrasonically bathed for 1 minute. When comparing, the figure set [15-20] to the FESEM imagery taken TNTs foils labelled; N11, N12, N13, s11, s12 and s12 the pore blockage caused by the electrolyte was removed.

The two electrolytes which were used were sol-gel based. The Ethylene Glycol based electrolytes ranged a concentration of 0.2, 0.5, and 0.7 wt% ammonium fluoride produced TNTs with varying results. The TNTs had varying lengths seen in SEM and FESEM results labelled s11, s12 and s13. The varying lengths suggests an issue with the dissolution of the TiO_2 ions. There seems to be a non-uniform concentration build-up of this dissolution process. The water content of the electrolyte was 10 wt% compared to the Glycol based electrolyte which had a ratio mix of 50:50, V: V. The viscosity of the Ethylene Glycol based electrolyte was much greater than the Glycol electrolyte. The fluid dynamics of the mixture seems to have resulted in this anomaly. The build-up of TiO_2 products from the dissolution process may not have been able to be cleared from the surface to allow for uniform nanotube development.

There was an issue which first occurred in the electrolysis of process of the synthesis of the TNTs. The TNTs pores were being developed into nanotubes and the electrolyte would fill the tubes to allow the process to continue. After the electrolysis process was completed the TNTs foils were taken to the annealing process. This order of electrolysis to annealing caused the electrolyte to be baked on to the surface and in the pores of the TNTs. This is seen the SEM figures, the SEM imagery showed the morphology being caked by the electrolyte the pores however can be seen underneath the electrolyte compound. The TNTs were placed in an ultrasonic bath to remove the remaining electrolyte from the TNTs. The process of ultrasonication was thought to destroy the nanotube structure as the FESEM imagery of the samples S11, S12 and S13 showed crushed and destructed nanotubes, it was then found the destruction of the opening of the tubes was not due to this as the TNTs developed in the Glycol solution showed no collapse of nanotubes after ultrasonication.

The process of optimisation of this project involved changing some of the steps in the fabrication and synthesis process. The main changes that took place where the introduction of autonomous voltage control, the change in electrolyte substrate, changes in the concentration of ammonium fluoride, changes in annealing temperature and sensitisation of the TNTs with the introduction of a nickel dopant species.

The introduction of the voltage program allowed for the reduction of human induced error in the synthesis process. The original synthesis process used a power supply with manual control to increase the voltage to a certain voltage over a given timeframe. The programable power supply involved coding a C++ executable and a python wrapper. The C++ executable was 708 lines and used Key stroke industries software to interpret VISA commands.

The synthesis method and testing method had many failures mainly introduced via failed reactions and incorrect use of equipment. The testing process of the degradation of rhodamine B uses a 300W Xeon lamp which produces a large amount of heat energy. This heat energy was causing the water in the Rhodamine B test solution to evaporate which lead to incorrect readings and progressively higher concentrations. To fix this issue the rhodamine B was placed into a condenser and a silicon glass plate was introduced to prevent evaporation.

The sensitization of the TNTs which was utilised was similar to the method prescribed by Huiong Li et al. With the change of the annealing process for baking under a Xeon lamp. The process was done to void building up nitrogen oxides on the surface which could damage the surface of the TNTs. The method of reducing the nickel hexahydrate by Sodium borohydride produceed excess hydrogen which were deemed unsafe given the scope of the project.

There was no need for a calibration curve for the use of the Spectrophotometer for the Rhodamine B analysis as the Initial concentration was measured and subsequently the differential of the concentrations was measured. Each set of data self originates as $\frac{C_0}{C_0} = 1$ and the rate of change can be analysed.

Catalyst characteristics

Morphology

The morphology of the TNTs varied from concentration and electrolyte. The average diameters of the TNTs produced with both electrolyte substrates was 100nm with a variance of 10nm. The hole diameters developed are similar sizes in all the TNTs fabricated this is caused by the voltage operation ranges. The initial voltage ramping and maximum voltage was set at 250mV/s and 20V's for all the electrolytes. This value was not changed due to the power supply in use.

The TNTs prepared with electrolyte comprised of ethylene glycol for the substrate has a comparatively unorganised and unstructured morphology when comparing it to the TNTs synthesised by an electrolyte with a Glycerol substrate. As the concentration of the ammonium fluoride increases the level over order in the nanotube arrays increases.

XRD

The XRD patterns in Figure 41 are taken from the most active photo catalyst which wish N13. N13 was then annealed at different temperatures to vary result of activity. The XRD patterns are very similar, from the phase diagram Figure 4 the ritual phase starts to occur at $350℃$, the temperature ranges which were varied where $400, 450\ and\ 550℃$. The XRD patterns for each of the samples are characterised by both phases which is validated by the phases state diagram. There are the characteristic peaks of $25°, 39°, 40,54°, 72°\ and\ 76°$ peaks. Sample labelled N13 share the same annealing temperature and have very similar peaks and peak heights. Each of the XRD patterns are highly representative of the pattern in Figure 45(b), the ritual peak of $27°$ does not appear in the XRD sample N13 $550℃$. The XRD analysis shows that there is a crystalline structure of anatase and ritual. In future, there should be a sample prepared at much higher temperatures where there is no anatase phase and the crystalline structure is homogeneously ritual. A temperature such as $800℃$ taken from Figure 4 there should only be a ritual crystalline structure. To perform further analysis the samples would have to be taken to a crystallographer.

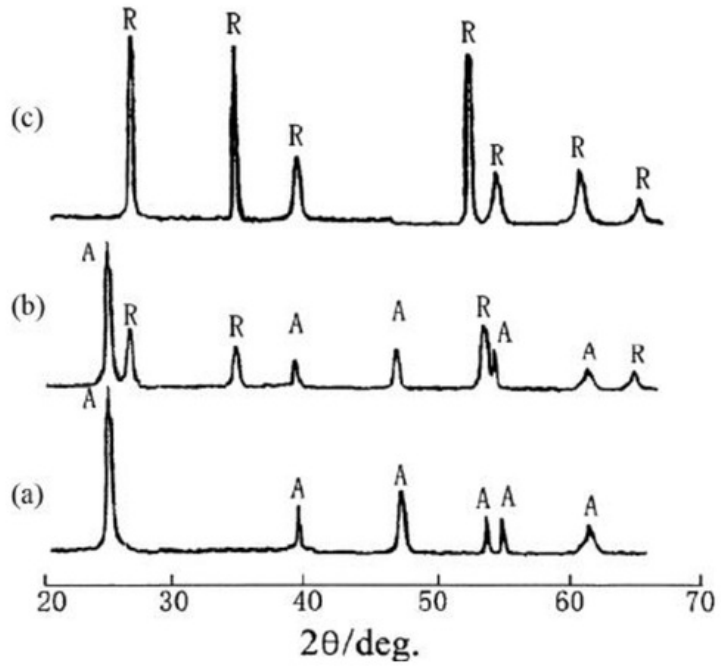

FIGURE 45 XRD PATTERN TIO2 ANATASE (A) , RITUAL (R) [20].

Catalyst Activity

The catalyst activity has followed the relationship discovered in previous studies. The main three variables which were changed where; electrolyte make, annealing temperature and decoration. There was however some discrepancy with the base chosen for the optimisation process.

The first test which was conducted in the experiment was the degradation of Rhodamine B with varying electrolyte seen in Figure 42. The degradation of Rhodamine B was first tested blank with Titanium foil as the photo catalyst. This black test showed that the Titanium foil alone had no or little effect as a photo catalyst. The degradation relationship that is observed is a linear relationship. The R^2 values for the line of best fit is 0.94 or greater. The blank R^2 values of 0.69 is an anomaly and the degradation seen was less than 1%. This 1% may have occurred in the measuring process as the spectrophotometer would have lost accuracy over each progressive measurement.

The most successful degradation from this sample was N13 with a degradation of 83.26%. This result can be correlated to the FESEM imagery. From Figure 40 to Figure 38 it is evident that N13 has the most ordered and arranged morphology. The trend when correlating the FESEM imagery and the degradation results shows that a more ordered structure has a greater photocatalytic effect. N11 and N12 show promise in order however taking images of different sections shows that there are sections where the nanotubes are destroyed or deformed.

A change in annealing temperature resulted a change in degradation. The most effective temperature was $450℃$. The highest temperature did not result in the highest degradation however showed greater degradation of rhodamine B then the lowest temperature. There may have been an error in testing as seen in Figure 43. The degradation of sample N13 $550℃$ has an anomaly at 20 minutes. The rate of N13 $550℃$ degradation seems to be like the N13 $450℃$ sample which could suggest that the N13 $550℃$ could have had a similar final degradation efficiency.

The decoration of the NiO via the Nickel nitrate hexahydrate method successfully deposited a nickel species on the surface of the TNTs as there was a clear difference of degradation efficiencies between a decoration with a solution concentration of 1mM/50mL of Nickel nitrate hexahydrate and 10mM/50mL. The decoration showed a similar relation to the other papers which showed over decoration could result in reduction of degradation efficiency a change from 54.20% to 49.06%. There was an anomaly where the blank N13 sample showed a much higher efficiency of 83.26%.

TABLE 5 SAMPLE DEGRADATION EFFECENECY.

Sample	Degradation %
N11	34.20
N12	69.70
N13 $400℃$	58.00
N13 $450℃$	83.26
N13 $550℃$	61.32
N13 1mM	54.20
N13 10mM	49.06
S11	63.38
S12	59.28
S13	61.14

Future work

There is much room for optimisation and improvement for the fabrication of TNTs. We will continue to see improvement in the application of TNTs in photovoltaics and photocatalytic applications. There are many doping species which could be use or as is or in combination to sensitize or co-dope/dope to improve the photocatalytic or photovoltaic capabilities. The main way to achieve this is to reduce the energy band gap requirement and increase the absorbance range of the electromagnetic spectrum.

The learning gap which was required to understand equipment and to obtain equipment training given this the improvement which could be made in future study could yield greater improvements. The greatest future improvements would be found in making the TNTs more ordered and uniform. Once the TNTs are highly ordered and the synthesis process produces products with the same accuracy and repeatability the TNTs could be tweeted and optimised to see relations clearer. The optimisation of TNTs with modification techniques such as doping and sensitisation with dopant species such as CdS Qds, N, S and C would prove great increases in efficiencies.

There was a lot of error in the reading of the degradation due to the uses of a portable spectrophotometer. Factors like evaporation and illumination errors could be constrained and removed with the development of custom testing rigs.

The application of photovoltaics shows more promise and is applicable to current economic and environmental needs. The degradation of Rhodamine B is very important for our environmental sustainability however the growing interest in photovoltaics the optimisation of TNTs for the photovoltaic application would provide greater translational value.

Conclusion

This study has discovered that the use of TNTs in a photocatalytic environment proves to be a very active photo catalyst. The electrolysis process is the most important process for the optimisation of TNTs in the specific application. The annealing, doping and sensitisation process are also very influential in the optimisation of TNTs. The introduction of NiO showed to influence the photocatalytic activity. The lowest degradation was found to be the N11 sample at 34% and the highest being the N13 sample at 84%.

The anomaly that was found regarding the N13 result may be caused as the synthesis of the three samples were done at different time frames however there is a clear relation between the order of the TNTs and the degradation efficiency. To Optimise the TNTs for the application of Rhodamine B would be to use an electrolyte substrate mix where there is an optimum viscosity, an electrolyte such as a Glycerol-water base and to have a fluoride ion supply to allow a uniform formation of nanotube arrays.

The ammonium fluoride concentration of 0.7wt% allowed for an optimised dissolution and mineralization rate so that the TNTs developed at a sustained rate. The viscosity of the electrolyte appears to have a great role in the removal of the mineralized ions to prevent nanotube structure deformation. An annealing temperature of $450℃$ and lightly sensitise the TNTs with Nickle oxide provided an increase in the degradation efficiency.

XRD, FESEM and SEM analysis proved to help the project by providing material and surface morphology characteristics. The degree of order in the TNTs was defined in the electrolysis process. The relationship of higher ordered TNTs showed higher photocatalytic activity.

The fabrication and synthesis of TNTs was successful. There was optimisation of the TNTs in the application of a photo catalyst to degrade rhodamine B however there is much more room for the optimisation of degradation of Rhodamine B with the use of a TNTs photo catalysts.

Bibliography

[1] S. IIJIMA, "Helical microtubules of graphitic carbon," *Nature, vol. 354, pp. 56 - 58,* 1991.

[2] S. B. Poulomi Roy and P. Schmuki*, "TiO2 Nanotubes: Synthesis and Applications," *Nanoscience,* 2011.

[3] H. T. J. M. M. P. S. Andrei Ghicov, "Titanium oxide nanotubes prepared in phosphate electrolytes," *Electrochemistry Communications, 7, 505 - 509,* 2005.

[4] J.M. Macak, H. Tsuchiya , A. Ghicov, K. Yasuda , R. Hahn, S. Bauer, P. Schmuki, "TiO2 nanotubes: Self-organized electrochemical formation, properties and applications," *Elsevier,* vol. 11, pp. 3-18, 2007.

[5] York R. Smith, Rupashree S. Ray, Krista Carlson , "Self-Ordered Titanium Dioxide Nanotube Arrays: Anodic Synthesis and Their Photo/Electro-Catalytic Applications," *materials,* 2013.

[6] w. J. H. P. Yongseok Jun and M. G. Kang*c, "The preparation of highly ordered TiO2 nanotube arrays by an anodization method and their applications," *ChemComm,* 2012.

[7] Janusz Nowotny, "Titanium dioxid ebased semiconductors for solar-driven environmentally friendly applications: impact of point defects on performance," *Energy & Environmental Science,* 2008.

[8] A. Murphy, "Does carbon doping of TiO2 allow water splitting in visible light? Comments on ''Nanotube enhanced photoresponse of carbon modified (CM)-n-TiO2 for efficient water splitting'',"* Solar Energy Materials & Solar Cells ,* vol. 92 , p. 363–367, (2008).

[9] H. G, "Comparison of dye- and semicondutor-sensitized porous nanocrystalline liquide junction solar cells," *J. Phys Chem C,* vol. 112, pp. 17778-17787, 2008.

[10] Yuxiang Zhua,b, Yanfei Wanga,*, Zhi Chenb,*, Laishun Qinb, Libin Yanga, Liang Zhua, Peng Tanga, Tong Gao b, Yuexiang Huang b, Zuoliang Shaa, Gao Tang b, "Visible light induced photocatalysis on CdS quantum dots decorated TiO2 nanotube arrays," *Applied Catalysis A: General,* vol. 498, p. 159–166, 2015.

[11] Huiong Li et al, "Constructing stable NiO/N-doped TiO2 nanotubes photocatalyst with enhanced visible-light photocatalytic activity," *Springer Science and Business,* 2015.

[12] W. D. SILVA, "Milestone in solar cell efficiency by UNSW engineers," UNSW newsroom, 17 May 2016. [Online]. Available: http://newsroom.unsw.edu.au/news/science-tech/milestone-solar-cell-efficiency-unsw-engineers. [Accessed 11 10 2016].

[13] O. K Varghese, D. Gong, M. Paulose, K. G. Ong and C. A. Grimes, "Sensors Actuators," *Sensors Actuators,* pp. 98,338, 2003.

[14] "A review and recent developments in photocatalytic water-splitting using TiO2 for hydrogen production," *Renewable and Sustainable Energy Reviews,* vol. 11, pp. 401-425, 2007.

[15] D. J. W. Gooch, Encyclopedic Dictionary of Polymers, vol. 15, Springer Link, 2009, p. 727.

[16] Jiandong Zhuang, Wenxin Dai, Qinfen Tian, Zhaohui Li, Liyan Xie, Jixin Wang, and Ping Liu*, "Photocatalytic Degradation of RhB over TiO2 Bilayer Films: Effect of Defects and Their Location," *American Chemical Society,* Vols. State Key Laboratory Breeding Base of Photocatalysis, Research Institute of Photocatalysis, Fuzhou University,, 2010.

[17] V. O. P. M. S. K. G. C. A. Mor G.K., "A review on highly ordered, vertically oriented TiO2 nanotube arrays: fabrication, material properties, and solar energy applications," *Sol. Energy Mater. Sol. Cells,* 2006,.

[18] Thillai Sivakumar Natarajan, Molly Thomas, Kalithasan Natarajan, Hari C. Bajaj, Rajesh J. Tayade∗, "Study on UV-LED/TiO2 process for degradation of Rhodamine B dye," *Chemical Engineering Journal,* no. 169, p. 126–134, 2011.

[19] Y. Z. Y. W. L. Z. L. Y. Xiaoyu Zhao and Z. Sha, "Influence of Anodic Oxidation Parameters of TiO2 Nanotube Arrays on Morphology and Photocatalytic Performance," *Nanomaterials,* 2015.

[20] H. Ijadpanah-Saravy a , M. Safari b , A. Khodadadi-Darban a & A.Rezaei , "Synthesis of Titanium Dioxide Nanoparticles for Photocatalytic Degradation of Cyanide in Wastewater," *Analytical Letters,* 2014.

[21] Y.-S. C. W.-M. H. Y.-C. C. Young Ku, "Effect of NH4F concentration in electrolyte on the fabrication of TiO2 nanotube arrays prepared by anodisation," *Micro \& Nano Letters,* 2012.

[22] P. S. Jan M. Macak, "Anodic growth of self-organized anodic TiO2 nanotubes in viscous electrolytes," *ScienceDirect,* 2006.

Appendix

Consultation Meetings Attendance Form

Week	Date	Comments (if applicable)	Student's Signature	Supervisor's Signature
2	12/8/16	Lab access/future Plans.	Mary	
3	16/8/16	reflection	Mary	Y. Wang
4	24/8/16	reflection - TNTAs images	Mary	Y. Wang
6	6/9/16	Direction	Mary	Y. Wang
6	9/9/16	Doping - band Gap	Mary	Y. Wang
7	13/9/16	RBS exp	Mary	Y. Wang
8	20/9/16	week Gap - RhB	Mary	Y. Wang
9	28/9/16	week Gap - RhB	Mary	Y. Wang
10	4/10/16	Ni / Co deposition	Mary	Y. Wang
11	11/10/16	Ni/Co deposition	Mary	Y. Wang
12	19			
13				

FIGURE 46 ATTENDANCE FORM.